Desalination and Water Treatment
www.deswater.com

doi: 10.5004/dwt.2021.27958

244 (2021) 90–109
December

Synthesis and characterization of novel forward osmosis thin film nano-composite membrane to enhance the reverse osmosis desalination economics

Ali M. Ismail[a,b,*], Yousra H. Kotp[b], M.G. Eloffy[a,c], A.H. Konsowa[a], Hosam A. Shawky[b]

[a]*Faculty of Chemical Engineering, Alexandria University, Alexandria, P.O. Box: 11753, Egypt, Tel. +201007134679; Fax: +2035902715; email: alimismail99@icloud.com (A.M. Ismail), Tel. +201226150501; email: manal_eloffy@yahoo.com (M.G. Eloffy), Tel. +201222162806; email: akonsowa@alexu.edu.eg (A.H. Konsowa)*
[b]*Egyptian Desalination Research Center of Excellence, Desert Research Center, Cairo, Egypt, Tel. +201063953608; email: yoso20002000@yahoo.com (Y.H. Kotp), Tel. +201002930710; email: hashawky@edrc.gov.eg (H.A. Shawky)*

[c]*National Institute of Oceanography and Fisheries, NIOF, Cairo, Egypt*

Received 28 May 2021; Accepted 2 November 2021

ABSTRACT

In this study, two main key features are used for the successful forward osmosis desalination process. The first key is the thin-film nanocomposite membrane fabrication. This key is achieved by consolidating different concentrations of zeolite nanoparticles in the polysulfone supporting sheet (ranging from 0%wt. to 0.6% wt.) to enhance the hydrophilicity and porosity of the membrane. A thin polyamide layer is formed on the top surface of the modified polysulfone by interfacial polymerization of Metaphenylenediamine (MPD) and Trimesoyl chloride (TMC) to fabricate thin-film nanocomposite (TFNC) forward osmosis membranes for forward osmosis (FO) application. The other key feature that makes the FO practical is selecting the ideal draw solute achieved by selecting sodium chloride as inorganic salt. Sodium chloride is characterized by high osmotic pressure, chemically inert, low membrane reverse solute flux, and easily regenerated. The fabricated TFNC membranes were first tested using a cross-flow RO module to evaluate the effect of different loadings of zeolite nanoparticles on the membrane performance. The FO membrane with 0.4 wt% zeolite in polysulfone matrix (TFNC-0.4%) shows the most promising results through increasing the water flux by 126% than the TFC membranes. Then were tested using a cross-flow FO module with 0.02–0.8 M NaCl concentration as feed solution. Results indicate that the water flux of the TFNC-0.4% was increased by (55%–64%) than the TFC Control membrane depending on the membrane orientation and draw solution concentration. It is observed that the solute reverse flux increased with the increase of the concentration of draw solution. Different characterization tests have been carried out on the forward osmosis membranes to verify their successful preparation and modification and specify the various effects of the zeolite nanoparticles added to the membrane substrate. A sponge-like structure is developed by adding zeolite nanoparticles compared to the TFC membrane, enhancing water permeability. Moreover, an increase in mechanical and thermal properties is detected. Furthermore, the power consumption for the forward osmosis process was [0.72–4.66%] only from the total power consumption of the FO-RO process. The current power cost as OPEX for FO TFNC-0.4% membrane desalination process ranges from 0.072 to 0.132 EGP/m^3 compared to the commercial SWRO+PX [5.53 EGP/m^3] operated in Hurghada, Red sea, Egypt.

Keywords: Forward osmosis; Zeolite nanoparticles; Thin film nanocomposite; Power consumption; Desalination

* Corresponding author.

1. Introduction

Nowadays, clean water scarcity has become a serious problem that threatens the national security of many countries, which will be aggravated due to exponential population growth [1]. In 2015, World Economic Forum in Davos ranked water scarcity problems as the most vital thread that will face humanity shortly. United Nations Food and Agriculture Organization (UNFAO) stated that by the year 2025, more than 66% of the world population would be underwater stress conditions, and more than 1.8 billion people will experience absolute water scarcity [i.e., <500 m^3/cap] [2]. Accordingly, water needs are in a logarithmic increase, and current freshwater resources may not meet human requirements. Egypt is one of the counties facing water scarcity and rapid population growth, which is a vital problem since the River Nile's freshwater is tremendously decreasing due to human activities. With the population expecting to double in the next 50 years and the negative impacts of the Grand Ethiopian Renaissance Dam (GERD) on the Blue Nile, the water shortage became a significant challenge for the Egyptian national security. Therefore, desalination could be considered a new source of freshwater along with the River Nile to solve Egypt's diversity of fresh water. Global water scarcity motivates water researchers to adopt new water sustainability strategies to develop new technologies for desalination and water treatment systems and enhance the current tactics for water production and distribution [3]. Seawater desalination is the most promising solution for this global threat as seawater represents more than 97% of the total water available on earth [1]. Water in form of brackish or seawater has been practiced regularly for over half a century as a sustainable water supply source in many counties [4].

For decades, aqueous separations have relied on hydraulic pressure in the form of reverse osmosis as the most economical solution for water desalination to drive water across membranes that retain suspended and dissolved solids. Even with energy recovery devices, a large amount of electrical power is required for high-pressure pumps to generate pressure for reverse osmosis plants that already have some drawbacks in terms of increasing energy prices and carbon footprint. While most water researchers focused on membrane science to enhance membrane properties in terms of higher permeability or higher rejection, minor efforts have targeted the separation driving force. Recently, water researchers spotlighted the osmotic pressure as an alternative natural occurring driving force for water desalination systems known as engineering osmosis or forward osmosis. In recent years, this alternative technology has gained potential as a solution for purification, desalination and power generation [5].

Engineering osmosis leans on natural occurring osmosis flow between aqueous solutions based on different osmotic forces that lead the pure flow from one key to another for various purposes. Two applications include forward osmosis desalination to produce purified low saline water: direct osmosis concentration (DOC) to concentrate valuable solutions by dewatering, and pressure retarded osmosis (PRO) to generate power by the flow kinetic energy. In both applications, the draw solution selection is the most important key component in driving the process with higher osmotic pressure properties based on the desired product [5].

Forward osmosis offers several advantages rather than other desalination technologies as it uses less expensive energy as it relies on osmotic pressure difference rather than electrical or thermal energy to drive water spontaneously across semi-permeable membranes. However, the energy type, quality, and quantity needed to depend entirely on the drawing solution selection and regeneration process. Forward osmosis offers very low fouling propensity rather than other hydraulically driven methods [6] due to the lack of compaction of the fouling layers, which occurs in NF/RO membranes, which are more resistant to chemical cleaning agents as the polyester dense support layer does not exist in the forward osmosis membranes. Another advantage of forward osmosis is that it does not require more power to increase the system recovery, as it just needs to increase the concentration of the draw solution to maximize the systems recovery without any risk of scaling potential due to the purity of the draw solution. Despite these strong points, forward osmosis still challenges the absence of a superior performance sustainable membrane and noble draw solution with excellent characteristics in terms of availability and economic regeneration [7].

Although the various advantages presented by the forward osmosis membranes in different water processes, water researchers adopt the idea of having a noble thin-film composite membrane with superior properties, especially at the top active skin layer under investigation. In 2012 Ma and Wei [8] prepared thin-film nanocomposite membranes TFN for water osmosis applications by incorporating zeolite nanoparticles into the top polyamide layer by interfacial polymerization of MPD and TMC monomers. The results showed that the optimized TFN membranes have higher water permeability than the typical TFC membranes by incorporating 0.1% wt/v of zeolite nanoparticles in the polyamide top layer. The improved water permeability is attributed to the newly created narrow size channel created by zeolite nanoparticles through which water molecules pass. In 2013 Liu and Qi [9] incorporated silver nanoparticles into the polyamide layer. Since thin-film composite forward osmosis membranes consist of a top selective layer and a microporous substrate layer, both layers could be optimized independently to enhance the forward osmosis performance [10]. In 2014 Emadzadeh incorporates titanium dioxide (TiO_2) nanoparticles in the substrate polysulfone layer with different concentrations ranging from zero to 1%. It was found that substrate hydrophilicity and porosity could be increased upon incorporating titanium dioxide in the membrane substrate. The improved water permeability is attributed to forming a finger-like structure in the substrate layer by increasing the TiO_2 concentration [11,12]. In 2020 Shawky incorporated silver nanoparticles in the polysulfone support layer that enhanced both water flux and salt rejection [13].

The main objective of the current work is to enhance reverse osmosis desalination economics by using forward osmosis as a promising technology process. Flat sheet thin-film nanocomposite (TFNC) forward osmosis membrane was synthesized and its performance was enhanced by adding zeolite nanoparticles to the membrane substrate.

Adding zeolite nanoparticles reduced the effect of internal concentration polarization, directly affecting the membrane flux rate. In addition, we studied the effects of zeolite nanoparticles loadings on the characteristics of PSF substrate and how the performance of the TFC is affected by those changes in the forward osmosis desalination processes. Moreover, we investigated the most efficient draw solution with the most optimum, economic, and feasible regeneration processes for seawater desalination in water flux and power consumption. The results of this research work are significant to exhibit that varying the PSF substrate's properties could be improved instead of changing the characteristics of the PA layer to enhance the FO membranes.

2. Materials and methods

2.1. Materials

Polysulfone Udel P-3500 LCD MB7 in pellets form (Solvay Advanced Polymer), dimethylformamide (DMF, >99.5%, Fisher Scientific), and polyvinylpyrrolidone (PVP K12, Acros Organics) were used for membrane substrate fabrication. M-phenyldiamine (MPD, >99%, Acros Organics), triethylamine (TEA, Fisher Scientific), camphor sulfonic acid (CSA, Sigma Aldrich), sodium lauryl sulfate (SLS, Adwic, Nasr Pharma), benzenetricarbonyl trichloride (TMC, >98%, Sigma Aldrich), n-hexane (>99%, Merck Millipore) for PA active layer synthesis. Zeolite nanoparticles with <21ηmparticle size (SSZ-73, Raatec) were used for enhancing substrate properties. Sodium chloride (NaCl, >99%, Adwic, Nasr Pharma) and Magnesium Chloride ($MgCl_2{\cdot}6H_2O$, >97%, Adwic, Nasr Pharma) were used for different concentration salt solution preparations for RO and FO experiments.

2.2. Preparation of flat sheet TFNC FO membranes

TFNC FO was prepared through two main steps: (1) preparation of polysulfone support membrane, and (2) preparation of TFNC active layer.

2.2.1. Preparation of polysulfone support membrane

Five substrates of different compositions were prepared using polysulfone dope solution, as presented in (Table 1). To prepare the dope solution, a specific concentration of zeolite nanoparticles was added at first to DMF, followed by a 60 min ultrasonication to reduce zeolite nanoparticles agglomeration. PVP was then added to the mixture under vigorous stirring on a hotplate for 15 min at 80°C. PSF pellets were then gently added to the solution under vigorous stirring for about 120–180 min until dissolving all polysulfone pellets. The prepared homogenous dope solution was then left at room temperature overnight to eliminate the trapped air bubbles within the prepared solution. The dope solution was then cast over a dry clean, thin glass platter by the automatic film applicator at a knife of 200 μm thickness, which was immediately placed into a water coagulation bath for the phase inversion process as shown in Fig. 1. Coagulation time has an essential effect on the preparation process [14]. Once the membrane was husked off from the thin platter, it was placed into an additional distilled water bath and stored overnight to eliminate any residual monomers to be ready for further experiments.

2.2.2. Preparation of TFNC FO membrane

The active barrier layer of the TFNC membrane was established by interfacial polymerization (IP) on the surface of the previously casted polysulfone substrate by using both aqueous and organic solutions; Tables 2 and 3. A solution of 50 ml of 2% (w/v) MPD aqueous solution was poured onto the top of the clamped substrate by the slope to remove any water residue and guarantee the MPD's permeation within the pores of the substrate. Then it was left for 2 min before disposing of the excess aqueous solution from the substrate surface. Tissue was used for cleaning the bottom of the membrane, and a rubber roller was used gently to remove any residual beads from the MPD from the surface of the substrate, as shown in Fig. 2. Then 50 ml of 0.53% (w/v) TMC organic solution was poured by the slope onto the clamped substrate layer to remove any residual from the MPD, leaving the clamped substrate for 1 min to ensure the completion of the interfacial polymerization (IP) process (Fig. 2). Then the excess of the organic solution was drained off and dried in the oven for 10 min at 80°C. The TFNC membranes were then stored in distilled water until they were tested. The formed TFNC FO membranes were abbreviated asTFNC-0.2%, TFNC-0.4%, TFNC-0.5%, and TFNC-0.6% according to the concentration of zeolite nanoparticles in the polysulfone support layer.

2.3. Membrane characterization

The synthetic forward osmosis membranes (control TFC and TFNC-0.4%) were characterized using different tools. The membrane morphology studies top surface and

Table 1
The composition PSF dope solution used for the FO membranes preparation

FO membrane samples	Composition of dope solution			
	PSF (wt.%)	PVP (wt.%)	DMF (wt.%)	Zeolite (wt.%)
TFC (Control)	17.5	0.5	82	0
TFNC-0.2%	17.46	0.5	81.84	0.2
TFNC-0.4%	17.43	0.5	81.67	0.4
TFNC-0.5%	17.41	0.5	81.59	0.5
TFNC-0.6%	17.39	0.5	81.51	0.6

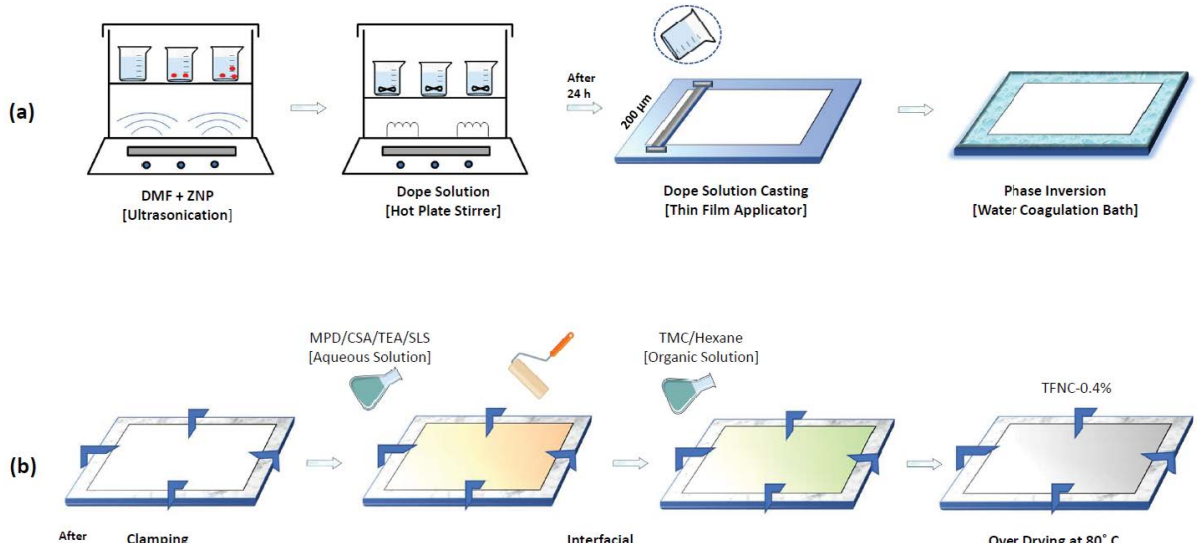

Fig. 1. (a and b) Schematic diagram for thin film nanocomposite membrane preparation.

Table 2
Composition of aqueous solution used in FO membrane polyamide layer

FO membrane samples	Composition of aqueous solution			
TFC/TFNC	MPD (wt.%)	TEA (wt.%)	CSA (wt.%)	SLS (wt.%)
	2	3	4	0.15

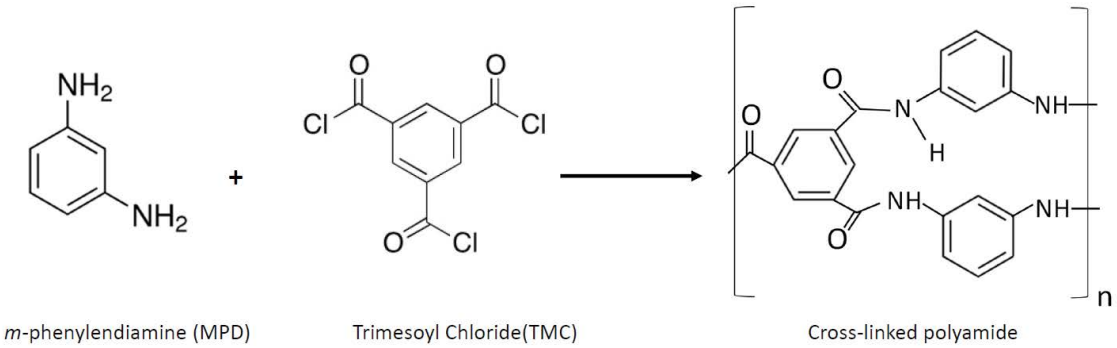

Fig. 2. Schematic representation of the intermolecular reaction between the TMC and MPD of polyamide layer.

cross-section of the (control TFC and TFNC-0.4%) were conducted using a scanning electron microscope (Quanta FEG-250, FEI) attached with Everhardt Thornley secondary electron detector (SED), with landing voltage range (standard 200 V to 30 kV), (beam deceleration of 20 V to 30 kV) and magnification 14 up to 1000000 x. The Electron optics is highly resolution Schottky field emission, and the SEM column is optimized for high brightness at high current. FTIR molecular spectroscope (Nicolet, 6700, Thermo Electron Corporation) was used to identify the functional groups of the membrane. The FT-IR equipped with smart beam splitter from quartz (27,000–2,800 cm^{-1}) to solid substrate (700–20 cm^{-1}) and detectors from silicon (27,000–8,600 cm^{-1}) to Si bolometer (600–20 cm^{-1}). X-ray diffractometer (Philips, X'pert, PANalytical) is used to investigate the variation in the polymer's crystalline nature that may occur by modifications and confirm the presence of zeolite nanoparticles within the substrate matrix.

Table 3
Composition of organic solution used in FO membrane polyamide layer

FO membrane samples	Composition of organic solution	
TFC/TFNC	TMC (wt.%)	Hexane (wt.%)
	0.53	99.47

The diffraction patterns were recorded using a copper (K) target with a secondary monochromator at 40 kV and 40 mA.

The knowledge of the thermal properties of materials is essential in determining their thermal stability, chemical and physical changes, characterization, and possibility of different applications. Thermal resistance is a description of the chemical stability of the polymer at high temperatures [15]. Thermo-gravimetric Analyzer (TGA-50, SHIMADZU) is used to conduct the TGA test from zero to 1,000°C with a heating rate of 10 deg/min (minute variations in mass can be detected). Dynamic mechanical analyzer (Q800, TA instruments, Kuleuven; force range 0.0001 N to 18 N; strain resolution 1 nm) was used to investigate mechanical properties for the membrane. Regarding the measurement of the porosity ε (%) of the membrane substrate, it was calculated from Eq. (1) by calculating the weight difference between the dry and wet membranes [11]. The dried membranes were stored in room temperature distilled water then weighted instantaneously after being primarily dried with a dry tissue. Where L is the membrane thickness, A is the membrane area, ρ is water density, W_w and W_d are membrane weight in dry and wet modes.

$$\varepsilon(\%) = \frac{W_w - W_d}{\rho_{H_2O} \times A \times L} \times 100 \tag{1}$$

2.4. Evaluation of membrane performance

2.4.1. Evaluation using RO experimental setup

The RO experimental setup scheme equipped with Sterlitech cross-flow RO membrane cell (CF042-RO) is represented in Fig. 3 to determine the prepared nanocomposite membrane's permeability and selectivity. The Sterlitech cell was 42 cm² as a total effective surface area. RO experiments were carried out using a solution of 1000 ppm as a feed solution at 4 bar, and the unit was operated with flow rate ranges between (2.5–3 L/min) with cross-flow velocities (0.32–0.39 m/s) respectively to minimize the concentration polarization. All experiments were performed after a membrane warming up that lasted for 60 min with distilled water. Moreover, all results were recorded after 2 h of operation until flux stabilization.

Permeate water flux (J_W^{RO}) (L/m² h) and water permeability (A) (L/m² h bar) [16] of the membrane were calculated using Eqs. (2) and (3) as below.

$$J_W^{RO} = \frac{\Delta V}{Am \times \Delta t} \tag{2}$$

$$A = \frac{J}{P} \tag{3}$$

where ΔV is the volume of the permeate, A_m is the membrane active surface area (m²), Δt is the time (h), and P is the membrane applied pressure (bar). The salt rejection (R) was determined according to Eq. (4).

$$R = \left(1 - \frac{C_p}{C_f}\right) \times 100 \tag{4}$$

where C_F and C_P are the concentration of feed and permeate (product) (ppm). (B) (L/m² h) is salt permeability coefficient [17] which is the intrinsic property of a membrane to reject salt was calculated based on Eq. (5), $\Delta\pi$ is the osmotic pressure difference across the membrane.

$$\frac{1-R}{R} = \frac{B}{A(\Delta P - \Delta\pi)} \tag{5}$$

2.4.2. Evaluation using FO experimental setup

The membranes that showed the best results in the RO experimental setup membranes were tested in two different operational modes. The active layer facing the feed water (AL–FW) is called the FO Mode, and the active layer facing the draw solution (AL–DS) is called PRO mode. Draw solution and feed water were pumped to the membrane

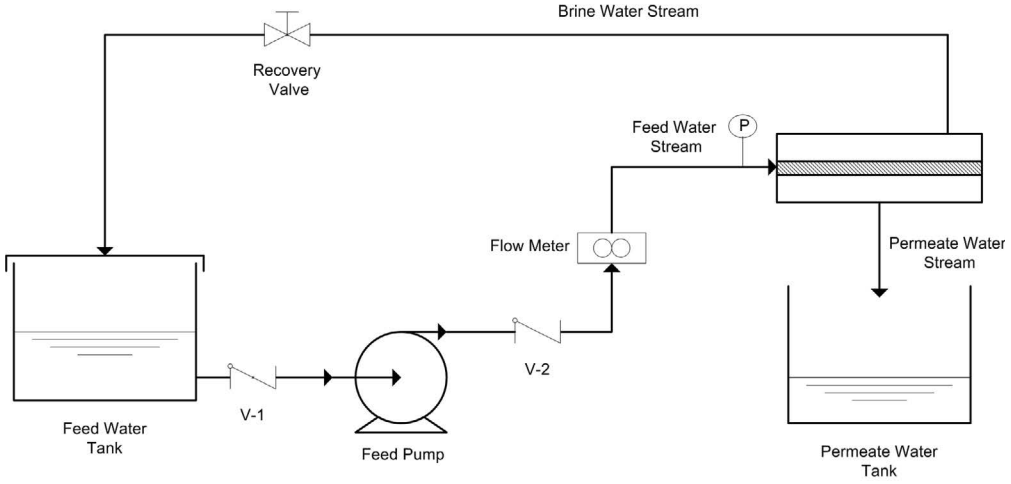

Fig. 3. Schematic diagram for the cross flow RO experimental setup.

cell in a countercurrent flow mode. Fig. 4 represents the FO experimental lab-scale setup scheme equipped with Sterlitech cross-flow FO membrane cell for the FO flat sheet membranes to determine the membrane water flux and the reverse solute flux. The FO Sterlitech was designed to have a 42 cm^2. The feed and draw solutions were circulated at a flow rate of 0.4 LPM with a variable speed pump (KNF 1300KT18RC and VI-3389, Fisher Scientific, respectively) to keep the flow rates aligned with the needed pressure, and the pressure was maintained at 6 psi (pressure gauges) using the feed and draw solutions concentrate valves during the process.

Both feed and draw solutions were kept within the room temperature 25°C. The draw solution tank was placed on a digital weighing balance to evaluate the pure water flux precisely. Both solution's salinities were measured by using a bench conductivity meter (3540, Jenway).

The draw solution tank was placed on a digital weigh balance to evaluate the pure water flux precisely. Both solutions salinities were measured by using a bench conductivity meter (3540, Jenway). All experiments were performed after a membrane warming up that lasted for 60 min with distilled water. Moreover, all results were taken after 30 min of operation until flux stabilization. After finish recording the water flux results, the weight balance was transferred to be under the feed water tank and run the unit for 30 min until the flux stabilizes then started to take the readings of the weight balance with respect to the feed solution conductivity changes within 20 min, knowing that each trial was made three times to yield an average value.

The FO water flux J_v (L/m^2 h) [12] was determined by measuring the weight change of draw solution according to Eq. (6):

$$J_v = \frac{\Delta V}{Am \cdot \Delta t} = \frac{\frac{\Delta m}{\rho}}{Am \cdot \Delta t} \tag{6}$$

where ΔV is the volume change of feed solution (L), A_m is effective membrane area (m^2), ρ is the density of feed solution (kg/m^3), Δm is the weight changes of feed solution (kg), and Δt is the measuring time interval (h).

After 30 min of the steady-state operation, the reverse solute flux J_s (g/m^2 h) [12] was calculated based on the salt concentration change by Eq. (7). Where; A_m is effective membrane area (m^2), Δt is the time interval (20 min), and C_t (mg/L) and V_t (m^3) are the salt concentration and the volume of the feed measured during the experiment.

$$Js = \frac{\Delta\left(C_t V_t\right)}{Am \cdot \Delta t} \tag{7}$$

In the FO experimental system, $NaCl/MgCl_2$ aqueous solutions with different low and high salinities concentrations were used as the feed/draw solutions. The osmotic pressure was calculated according to Eq. (8) (Van't Hoff equation):

$$\Pi = i\text{MRT} \tag{8}$$

where π is the osmotic pressure in (atm), i is the Van't Hoff Constant, M is the molarity of the aqueous solution, R is the universal gas constant (0.08206 L atm/mol K), T is the feed and draw solutions temperatures (K). In addition to J_v and J_s, the FO power consumption is evaluated using Eq. (9),

$$E_{S-\text{FO}} = \frac{1}{\left(36 \times \eta \times Q_p\right)}\left(P_f Q_{\text{SW}-in} + P_{\text{ds}} Q_{\text{ds}-in}\right) \tag{9}$$

where Es-FO (kWh/m^3) is the specific power consumption for the forward osmosis process, η (%) is the pump efficiency, P_f (bar) is the feed solution pressure, P_{ds} (bar) is the draw solution feed pressure, Q_p (m^3/h) is the permeate flow rate and $Q_{sw\text{-}in}$ and $Q_{ds\text{-}in}$ are the inlet flow rates for feed water and draw solution, respectively [18]. In addition, the total power consumption for the FO-RO is evaluated using Eq. (10):

$$E_{st} = E_{\text{S-RO}} + E_{\text{S-FO}} \tag{10}$$

where the E_{st} (kWh/m^3) is the total power consumption of both FO/RO processes and Es-RO (kWh/m^3) is the specific power consumption for the reverse osmosis calculated using ROSA software.

3. Results and discussion

3.1. Characterization of TFC and TFNC FO membranes

The morphology of the top surface and cross-section of the prepared TFC and TFNC-0.4% membranes were

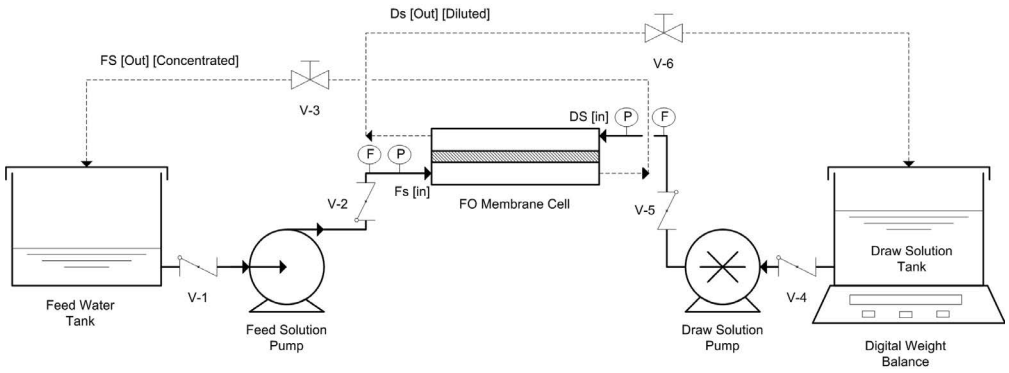

Fig. 4. Schematic diagram for forward osmosis membrane experimental setup.

examined using a scanning electron microscope. The TFNC-0.4% membrane had the same ridge-and-valley structure as the TFC membrane. At a high magnification of 20,000, deposits of bright nanoparticles can be detected on the membrane surfaces. The presence of zeolite nanoparticles in the main membrane structure increases membrane porosity as the number of pores increases in the TFNC-0.4%, as shown in Figs. 5a and b [19,20]. The cross-section views of the TFC and TFNC-0.4% membranes are shown in Figs. 6a and b. These SEM images show that the sponge-like macro-voids extended from the bottom to the top of the substrate layer (The overall thickness of the substrates was in the range of 100–130 μm). Compared to the pure polysulfone (PSF) substrate, the existence of hydrophilic zeolite nanoparticles in the dope solution greatly promotes water diffusion from the water coagulation bath to the casted polysulfone film, resulting in the development of more sponge-like pores, which facilitates the water flow and enhance the overall porosity that in turn plays a significant role in increasing the water flux [19,20]. Moreover, it could be noticed that there are two sponge layers in the membrane substrates, a high-dense sponge layer, and a lower dense layer compared to the pure polysulfone dope solution. The existence of hydrophilic zeolite nanoparticles in the PSF decreases the higher denser sponge layer from 35 to 9 μm, which directly affects the substrate's overall porosity. The sponge-like skin layers of the substrates were responsible for providing a smooth surface and sufficient mechanical cushion for the polyamide rejection layers. As shown in the SEM images (Fig. 5), for TFNC, the presence of hydrophilic zeolite nanoparticles within membrane substrate (PSF) decreases the higher denser sponge layer from 35 to 9 μm leads to the formation of large number of interconnected small pores that increases the mass transfer area for osmotic flow to take place in the membrane substrate [21–24]. Which in turn increase the membrane porosity and wettability thus leading to enhanced flux rates and performance stability. Leading to the reduction of the internal concentration polarization (ICP). Also, some agglomerations of zeolite nanoparticles (small white spots on SEM image) are formed at the cross-section of TFNC-0.4% membrane due to interaction between zeolite nanoparticles with polyamide. [19–25].

FTIR molecular spectroscope was used to identify the functional groups of the TFC and TFNC-0.4% membranes. As shown in Fig. 7 for the TFC, the peaks at the specific wave number of 1,151~1,155 cm^{-1} (symmetric O=S=O stretching), 1,294~1,295 cm^{-1} (asymmetric O=S=O stretching), 1,240~1,258 cm^{-1} (asymmetric C–O–C stretching), 1,486~1,490 cm^{-1} (CH_3–C–CH_3 stretching) and 1,490 cm^{-1} (C=C aromatic ring stretching) are conformed to polysulfone substrate functional groups [26–28]. Regarding the polyamide layer the characteristic peaks are 1,664~1,668 cm^{-1} (C=O amide stretching) and 1,581 cm^{-1} (C–N amide stretching) [28–31] and this is considered for both TFC and TFNC membranes. While the zeolite characteristic peaks at 1,014 cm^{-1} (Si–O stretching), 918 cm^{-1} (Al–OH bending), 569 cm^{-1} (Si–O–Al bending), and 463 cm^{-1} (Si–O–Si bending) are corresponded to the functional groups of zeolite nanoparticles [32].

X-Ray diffractometer is used to explore the transform in the crystalline nature of polymers that may occur by modifications and confirm the presence of zeolite nanoparticles within the substrate matrix. Fig. 8 shows the XRD patterns of the TFC, TFNC-0.4%, and pure zeolite nanoparticles. From the XRD pattern, it was clear that TFC membranes are mainly amorphous in nature and have one prominent peak at around $2\theta = 17$, on the other side in the TFNC-0.4% membrane, we can find some characteristics peaks at $2\theta = 29$, 36, 39.5, 48.3 and 64.5 in addition to mainly amorphous peak at around $2\theta = 17$ which reflects the crystalline nature of zeolite in the polysulfone substrate. Therefore, when comparing the TFC and TFNC-0.4%, X-ray diffraction patterns, it is clear that a remarkable increase in the degree of crystallinity in the TFNC due to the interaction of zeolite nanoparticles with polysulfone. In addition to that, we can find the zeolite nanoparticles patterns that are mainly crystalline in nature at $2\theta = 8.8$, 9, 11.2, 13, 17.4, 22.5; these results correspond to the pattern of zeolite nanoparticles [20].

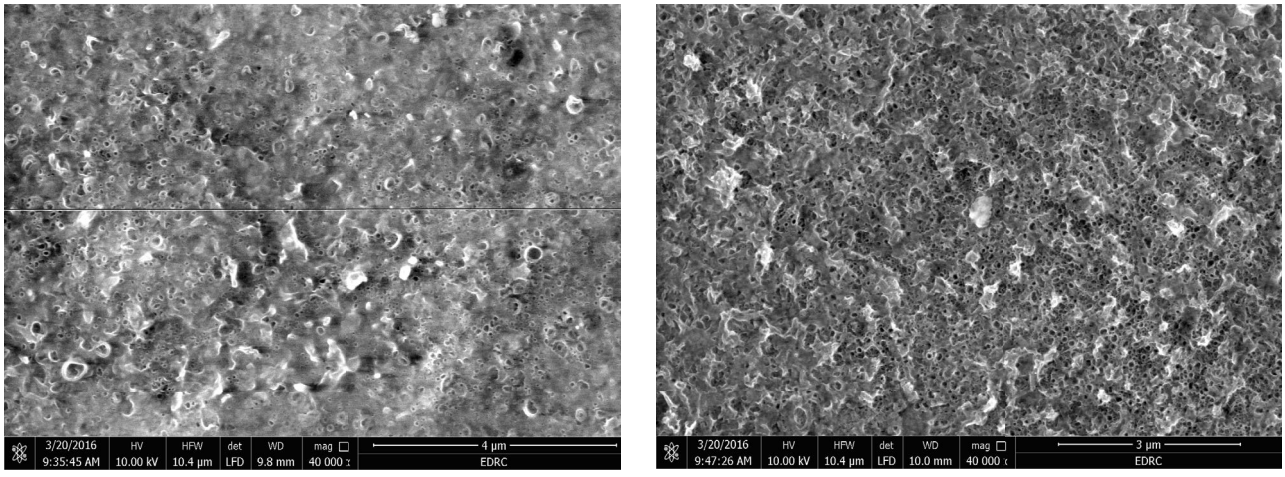

[a] **[b]**

Fig. 5. (a and b) SEM images for TFC and TFNC-0.4% membrane top surface.

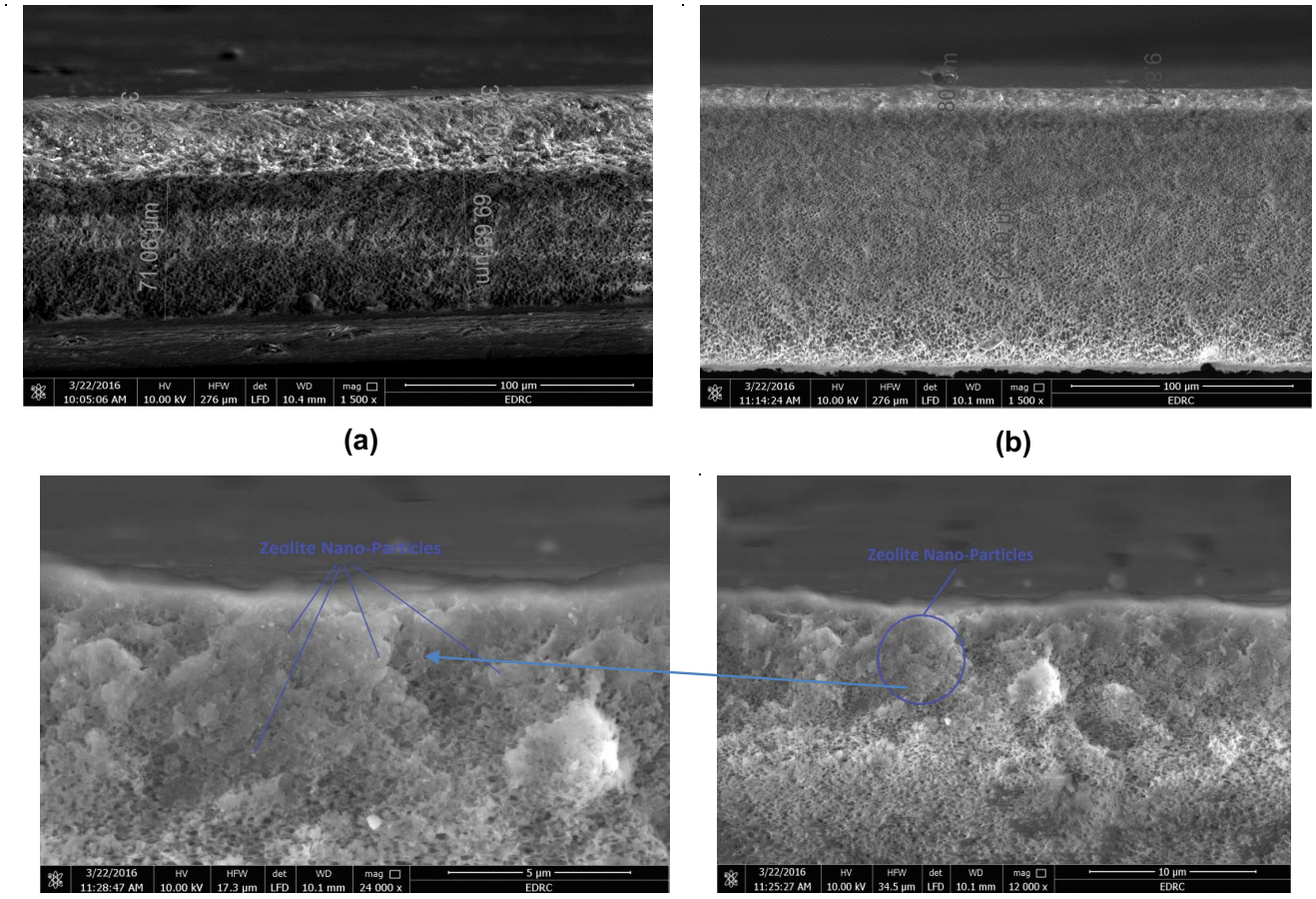

Fig. 6. (a and b) SEM images for the TFC and TFNC-0.4% membrane cross section.

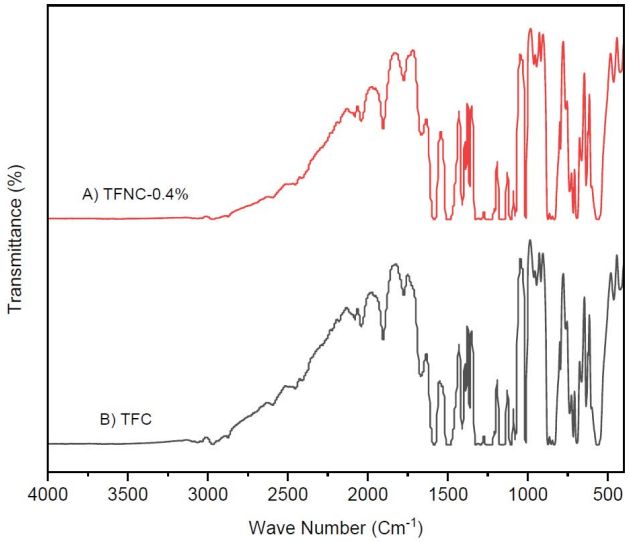

Fig. 7. FTIR spectra of (a) TFNC-0.4% zeolite membrane and (b) TFC membrane.

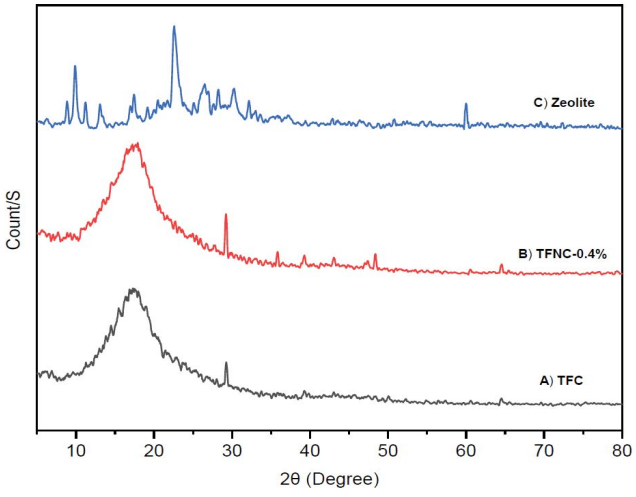

Fig. 8. XRD diffraction pattern of: (a) TFC, (b) TFNC-0.4%, and (c) zeolite nano-particles.

TGA is used to determine the fabricated membrane thermal stability Fig. 9 shows the weight loss (degradation) in the TFC occurred in two steps at midpoint 536.28°C by 46.52% and at midpoint 705.86°C by 32% with a total overall weight loss of 79%, which is higher than TFNC-0.4% zeolite modified membrane in which the weight loss occurs in three steps at midpoint 345.35°C by 2.12%, at midpoint 524°C with 31.15% and midpoint 678°C with total weight loss 39.35% with overall total weight loss 72%.

The 32% weight loss occurs in TFC membrane above 705.86°C related to polymer main chain splitting resulting in the final material, carbon, obtained at more than 600°C [33,34]. The reasons for the TFNC-0.4% membrane stability is expected to arise primarily from these chemical structures, composed of high-temperature resistance building units, such as amide groups and benzene rings [35]. While, sharp loss above 678°C is related to the polymer main chain splitting and the formation of zeolite oxide. It is observed that the weight loss of the TFN-0.4% is less than weight loss in the TFC membrane, which improves the thermal stability in the nanocomposite membrane. This improvement may be attributed to the interaction of coordinate bonds, covalent bonds, Van Der Waals forces, or hydrogen bonds between zeolite nanoparticles and polymeric chains [36]. These restrict the thermal action of macromolecules, increase the rigidity of the macromolecular chain, and enhance the energy needed by the polymeric chain movement and breakage, thereby promoting the membrane thermal properties [11,37–42].

Dynamic Mechanical Analyzer was used to investigate mechanical properties for the membrane. To evaluate the material's intrinsic and extrinsic mechanical properties, deformation is performed on a membrane sample, where sinusoidal stress or strain is applied to the material, and the resultant sinusoidal strain or stress is measured. As shown in Fig. 10; the mechanical properties of the TFNC-0.4% (stress/strain 10.34 MPa, 15.46%) membrane increased compared to the TFC (stress/strain 8.57 MPa, 13.88%) membrane, which could be attributed to the presence of the zeolite nanoparticles that increased the mechanical properties of the membrane [19,20,38].

Regarding the measurement of the porosity ε (%) of the membrane substrate, it was noticed that the overall porosity of the membrane increased from 62% for the TFC membrane to 65.6% for the TFNC-0.4%. This increase could be attributed to the addition of the zeolite nanoparticles that increased the membrane porosity, decreasing the structural parameter S that minimizes the internal concentration polarization during the FO processes that increase water permeability [19,43,44].

3.2. *Effect of zeolite loadings on the performance of TFNC membrane for RO experiments*

In Fig. 11 the comparisons between TFC and TFNC-0.4% prepared membranes were conducted among the separation performances. The water flux of the fabricated FO membranes increased sequentially with the zeolite nanoparticles content increase in the PSF sheet. The enhanced TFNC-0.4%illustrates a 126% increase in water flux rate with 3.21 L/m^2 h compared to the control TFC membrane 1.42 L/m^2 h under test conditions of 4 bar using 1 g/L of sodium chloride feed solution. This increase could be attributed to the enhanced substrate hydrophilicity and the increased overall porosity upon adding zeolite nanoparticles [19,20]. The rejection of NaCl into polyamide layers is attributed to zeolite nanoparticles incorporation. The retention percentage of the prepared membranes was linked with special compositions of zeolite nanoparticles in the PSF matrix. Thus, as seen in Fig. 11, the salt rejection percentage of sodium chloride was determined to be 91.03% and 96.7% for TFC and TFNC-0.4%, respectively, when 0.4% wt. of zeolite nanoparticles were embedded into the PSF matrix.

Furthermore, when loading more zeolite nanoparticles from 0.5% wt. to 0.6%wt., the corresponding rejection decreased to be 94.9% and 94.3% to TFNC-0.5% and

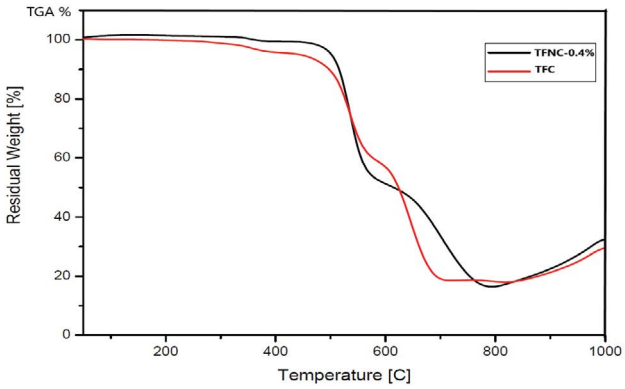

Fig. 9. TGA for both TFC and TFNC-0.4% membranes.

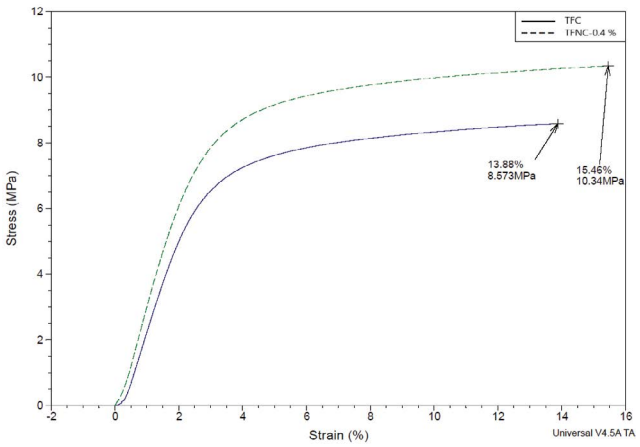

Fig. 10. Stress/strain curve for both TFC and TFNC-0.4% membranes.

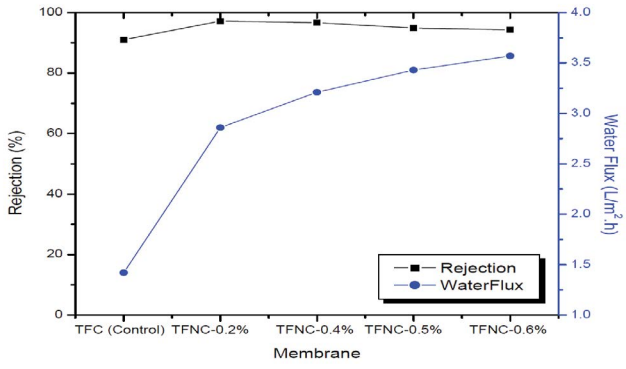

Fig. 11. Water flux and NaCl rejection of TFC and TFNC membranes prepared from different types of PSF substrates (Test condition 4 bar, 25°C and 1,000 ppm NaCl aqueous solution).

TFNC-0.6% membranes, respectively. This relative decrease in the salt rejection may be due to the aggregations of zeolite nanoparticles at high concentrations, leading to form non-selective boundaries and cavities between NPs and PA matrix [44,45].

Therefore, the TFNC-0.4% membrane was used for FO experimental setup as it shows the most balanced results between the flux (0.81 L/m² h bar) and salt rejection (96.7%) among the other TFNC membranes. The water permeability of the synthesized TFNC-0.6% membrane is (A = 0.91 L/m² h) as seen in Table 4; this value is three times higher than the commercial CTA-W membranes (A = 0.303 L/m² h) and is two times higher than the commercial CTA-NW membrane (A = 0.46 L/m² h) [46]. It could be noticed that the TFNC membranes outperformed the CTA commercial membranes as the Zeolite nanoparticles play a significant role in enhancing TFC membrane performance. Therefore, it could be more applicable than the CTA membranes in commercial applications that exhibit low permeability and high salt passage [19,46–50]. In addition to their limited PH operating range that needs extra chemicals for PH adjustment. Moreover, The stability of the TFNC-0.4% membrane was tested using a time stability test with 1,000 ppm NaCl feed solution at 4 bars, as shown in Fig. 12. It can be observed that the TFNC-0.4% exhibits good stability properties with respect to permeate flux and salt rejection for more than 30 h.

3.3. *Effect of zeolite loadings on the performance of TFNC membrane for FO experiments*

The influence of zeolite loadings on pure water flux and reverse solute flux were determined by FO cross flow experimental setup. The experiments were performed using a range of water salinities from brackish water to seawater as feed water prepared in the laboratory. Different solutions of 0.4 $MgCl_2$ [80,000 ppm-29 bar], 1.2 M NaCl [70,000 ppm-60 bar], and 2 M NaCl [120,000 ppm-101 bar] were used as a suggested draw solutions with different high concentrations. Results stated that the TFNC modified polysulfone substrate membranes presented a much higher flux for both orientations regardless of changing the draw solutions or changing in feed water salinities compared to the TFC membrane. This higher flux minimizes the resistance against water permeation due to the improved structural properties of the polysulfone substrate.

As shown in Fig. 13a, the TFNC-0.4% membranes outperformed the TFC (control) membranes across a wide range of different water salinities by using the sodium chloride as a draw solution; as the membrane water flux increased by 80% from 15.87 L/m² h for TFC to 28.5 L/m² h for TFNC-0.4% in AL-DS (for 1.2 M NaCl draw solution vs. 500 mg/L feed water). Also, it was increased by 78% from 8.73 L/m² h for TFC to 15.6 L/m² h for TFNC-0.4% in AL-DS (for 1.2 M sodium chloride draw solution vs. 45,000 mg/L feed seawater).

Similarly, as shown in Fig. 13b, the membrane pure water flux increased by 79% from 9.2 L/m² h of TFC to 16.5 L/m² h of TFNC-0.4% in AL-FW. Also, it was increased by 76% from 5 L/m² h for TFC to 8.88 L/m² h for TFNC-0.4% in AL-FW (1.2 M sodium chloride draw Solution vs. 45,000 mg/L feed water).

As stated from Fig. 14a, the same increasing trend was also observed as the TFNC-0.4% membrane outperformed the TFC membranes across a wide range of different water salinities by using the sodium chloride (NaCl) as a draw solution, as the membrane water flux increased by 79.8% from 27.1 L/m² h for TFC to 48.6 L/m² h for TFNC-0.4% in AL-DS (2 M sodium chloride draw solution vs. 500 mg/L feed water). Also, it was increased by 80% from 18.2 L/m² h for TFC to 32.7 L/m² h for TFNC-0.4% in AL-DS (2 M sodium chloride draw solution vs. 45,000 mg/L feed water). Similarly, as can be seen from Fig. 14b, that the membrane water flux increased by 78% from 15.6 L/m² h for TFC to 28 L/m² h for TFNC-0.4% in AL-FW (2 M sodium chloride draw solution vs. 500 mg/L feed water). Also, it was increased by 81% from 10.2 L/m² h for TFC to 18.4 L/m² h

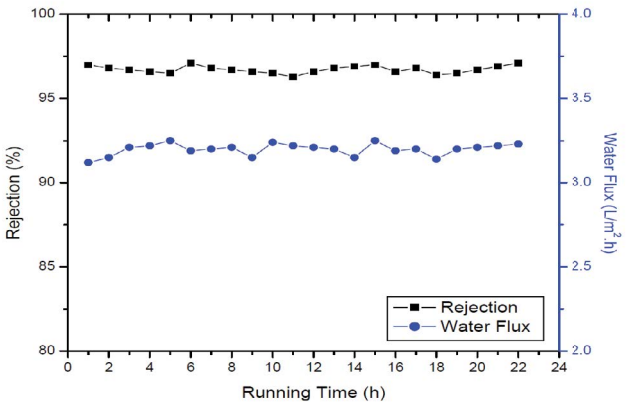

Fig. 12. Stability Test of TFNC-0.4% membranes. (Test condition 4 bar, 25°C and 1,000 ppm NaCl aqueous solution).

Table 4
Comparison between the separation properties of TFNC membranes in this work and commercial CTA membranes

FO membranes	Separation properties of TFNC and commercial CTA membranes	
	Water permeability (A) (L/m² h Bar)	Salt permeability (L/m² h)
TFNC-0.4% [This Work]	0.81	0.087
TFNC-0.5% [This Work]	0.86	0.091
TFNC-0.6% [This Work]	0.91	0.096
CTA-W [38]	0.303	N/A
CTA-NW [38]	0.46	N/A

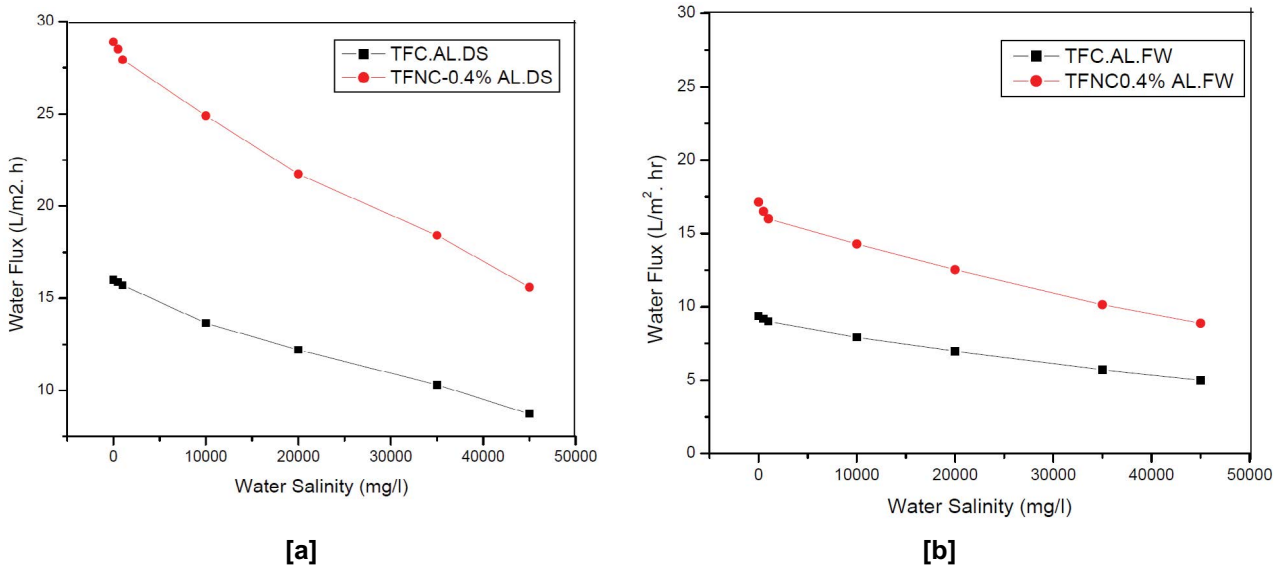

Fig. 13. (a and b) Water Flux for both TFC and TFNC-0.4% membranes (Test condition: 6 psi, 0.4 lpm, 25°C (AL-DS/FW) (draw solution 1.2 M NaCl).

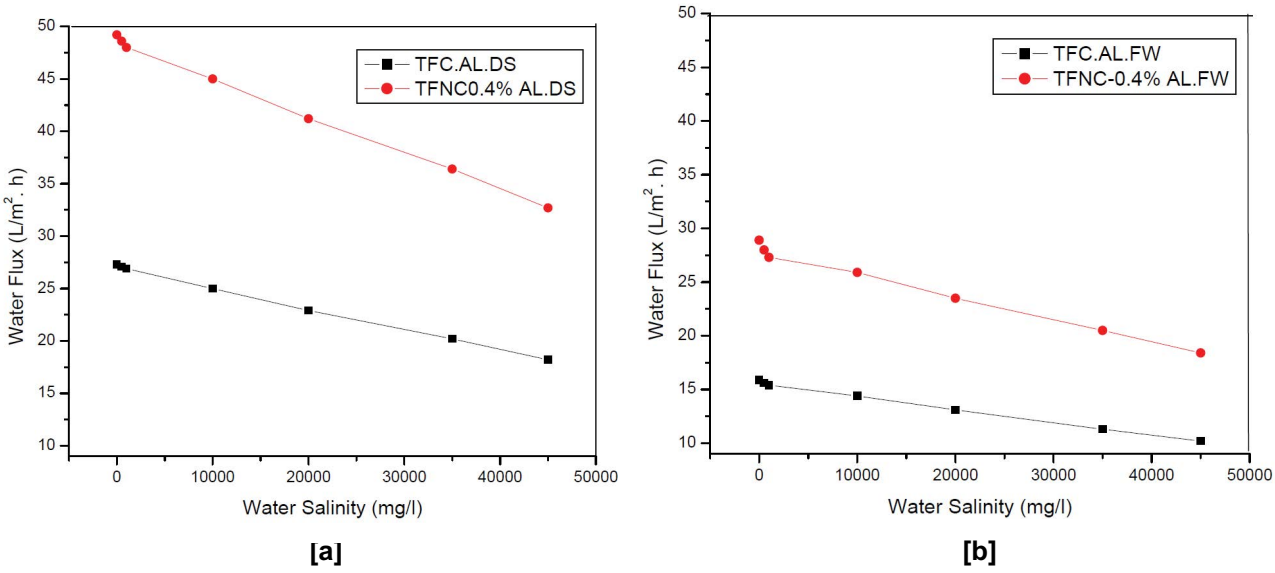

Fig. 14. (a and b) Water Flux for both TFC and TFNC-0.4% membranes (Test condition: 6 psi, 0.4 lpm, 25°C (AL-DS/FW) (draw solution 2 M NaCl).

for TFNC-0.4% in AL-FW (for 2 M sodium chloride draw solution vs. 45,000 mg/L feed water).

The same increasing trend in water flux was observed between the TFC and the TFNC membranes with respect to the different membrane orientations and increasing in feed salinities when increasing the draw solution concentration of NaCl from 1.2 M to 2 M. This may be attributed to the greater osmotic driving force available when a draw solution of higher concentration is used [19], that is, the higher the difference in osmotic pressure between the draw solution and feed water the higher the water flux that could be achieved.

Another draw solution was also investigated as a potential draw solution. As stated in Fig. 15a, the TFNC-0.4% membrane outperformed the TFC membranes across a wide range of different water salinities by using the magnesium chloride ($MgCl_2$) as a draw solution. The membrane water flux increased by 76% from 7.93 L/m^2 h for TFC to 13.96 L/m^2 h for TFNC-0.4% in AL-DS (0.4 M $MgCl_2$ draw solution vs. 500 mg/L feed water). Also, it was increased by 60% from 2 L/m^2 h for TFC to 3.17 L/m^2 h for TFNC-0.4% in AL-DS (0.4 M $MgCl_2$ draw solution vs. 25,000 mg/L feed water). Similarly, as shown from (Fig. 15b), the membrane water flux increased by 72% from 4.76 L/m^2 h for TFC to 8.2 L/m^2 h

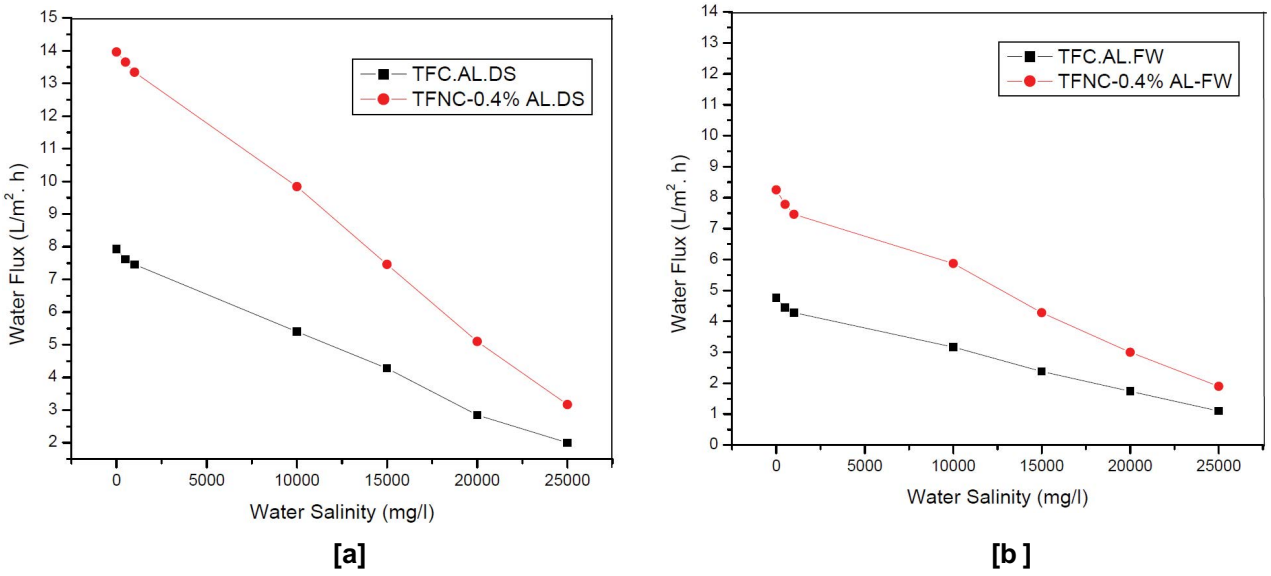

Fig. 15. (a and b) Water Flux for both TFC and TFNC-0.4% membranes (Test condition: 6 psi, 0.4 lpm, 25°C (AL-DS/FW) (draw solution 0.4 M $MgCl_2$).

for TFNC-0.4 in AL-FW (0.4 M $MgCl_2$ draw solution vs. 500 mg/L feed water). Also, it was increased by 74% from 1.1 L/m² h for TFC to 1.9 L/m² h for TFNC-0.4% in AL-FW (0.4 M $MgCl_2$ draw solution vs. 25,000 mg/L feed water).

The same increasing trend in water flux was observed between the TFC and the TFNC membranes regarding the different membrane orientations and increasing feed salinities. It was noted that the magnesium chloride practical solubility limit is very low as it reaches a maximum concentration of 80,000 mg/L (0.4 M) $MgCl_2$. Moreover, it provides a very low osmotic pressure (29 bar) at this point. As a result, it shows lower fluxes when used as a draw solution than the sodium chloride due to the decreasing of the osmotic pressure difference between the magnesium chloride and the feed water. Other divalent salts were evaluated, such as calcium chloride ($CaCl_2$) and magnesium sulfate ($MgSO_4$) but, they showed a very low osmotic pressure and solubility limit compared to the sodium chloride. Therefore it has been proven that improving the characteristics of polysulfone substrate could be a more practical approach rather than enhancing the polyamide layer characteristics by incorporating zeolite nanoparticles in the membrane substrate for the internal concentration polarization minimizing [11,47].

The membranes' solute fluxes were tested at different orientations, as shown in Fig. 16. It must be stated out that there was a significant increase in solute flux in TFNC-0.4% (13 g/m² h) in AL-DS mode and 4.6 g/m² h in AL-FW mode compared to control TFC membrane (6.04 g/m² h) in AL-DS mode and 2.3 g/m² h in AL-FW mode respectively when using 2 M NaCl as a draw solution. Similarly, in using 0.4 $MgCl_2$ as a draw solution, a significant increase in solute flux in TFNC-0.4% (3.2 g/m² h) in AL-DS mode and 1.7 g/m² h in AL-FW mode compared to control TFC membrane 1.5 g/m² h in AL-DS mode and 0.42 g/m² h in AL-FW mode respectively.

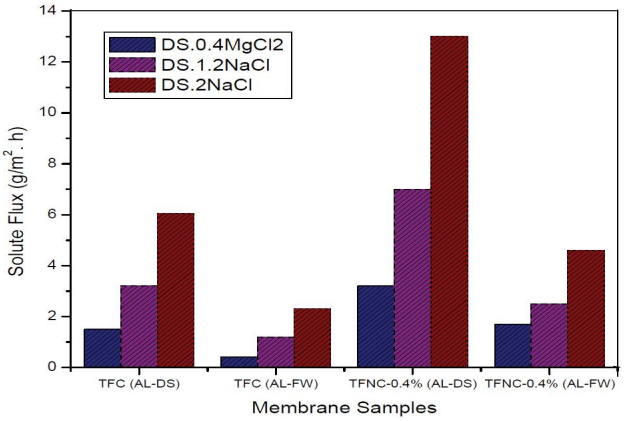

Fig. 16. Reverse solute flux for both draw solutions for both TFC and TFNC-0.4% membranes at different orientations (Test condition: 6 psi, 0.4 lpm, 25°C) (feed water, distilled water).

Eventhough the water fluxes of TFNC-0.4% membranes were remarkably improved, It was noticed that the reverse flux is higher in using the NaCl as a draw solution. This behavior could explain that the high concentration of draw solute at the support layer-active layer interface is crucial for developing a higher osmotic pressure gradient, which drives a higher water flux. However, this higher concentration from the draw solute also increases the concentration gradient across the active layer, increasing the reverse salt flux. Moreover, it was noticed that the AL-DS membrane orientations have higher reverse solute flux than that of the AL-FW, possibly due to increasing water flux that increases the solute reverse flux. Tables 5 and 6 state a comparison between membranes performance with other works with different membrane orientations. It could be noticed that the water flux and reverse

Table 5
Comparison between FO membranes performance (AL-DS)/PRO

FO membranes	Comparison between FO membranes performance [AL-DS]/PRO			
	Water flux (L/m² h)	Reverse salt flux (g/m² h)	Feed solution	Draw solution
TFC [This Work]	27.3	6.04	2 M NaCl	DI
TFNC-0.4% [This Work]	49.1	13	2 M NaCl	DI
TFC [11]	32.3	14.2	2 M NaCl	DI
TFN0.6 [11]	59.4	31	2 M NaCl	DI
sPPSU [39]	54	8.8	2 M NaCl	DI
SPSF [40]	47.5	12.4	2 M NaCl	DI

Table 6
Comparison between FO membranes performance (AL-FW) FO

FO membranes	Comparison between FO membranes performance [AL-FW]/FO			
	Water flux (L/m² h)	Reverse salt flux (g/m² h)	Feed solution	Draw solution
TFC [This Work]	15.9	2.3	2 M NaCl	DI
TFNC-0.4% [This Work]	28.9	4.6	2 M NaCl	DI
TFC [12]	13.9	5.3	2 M NaCl	DI
TFN0.6 [12]	33	15.7	2 M NaCl	DI
sPPSU [40]	48	7.6	2 M NaCl	DI
SPSF [41]	26	8.3	2 M NaCl	DI

solute flux are lower in ourwork compared to the work of Emadzadeh et al.[12]. This decrease may be attributed to the difference in the membrane support morphology;our work's membrane support morphology is sponge-like support compared to finger-like support in Emadzabeh's work. Although substrates with more pores facilitate water flow, wide pore leadsto a high water flux witha high salt leakage (i.e., high reverse solute flux) [48], that is why the finger-like membrane support has a higher reverse salt flux compare to the sponge-like membrane support.

In all practical results in our work and all previous works, the PRO membrane orientation (AL-DS) mode outperforms the FO membrane orientation (AL-FW) in terms of water flux and salt retention. This is attributed to the lower concentrative internal concentration polarizationfor PRO mode. Where salts are gradually accumulated within the porous support membrane layer due to diffusion of pure water towards the draw solution sucked from the feed solution due tothe osmotic pressure gradient.On the other side, the dilutive internal concentration polarization takes place in the FO mode. Where osmotic solutes are diluted even before flux can happen within the porous support membrane layer due to diffusion of pure water towards the draw solution withdrawn from the feed solution as a result of the osmotic pressure gradient.Therefore, the PRO membrane orientation mode is preferred when the feed solution is a lower molecular weight compound, andthe FO membrane orientation mode is preferred when the feed solution is higher molecular weight compounds that lead to the increased osmotic pressure gradient that yields higher flux rates [51–53]. Higher molecular weight compounds may lead to cake formation within the porous support membrane layer due to shear forces reduction and inhibit back diffusion [54].

The specific reverse solute flux diffusion (J_S/J_V), which refers to draw solutes leakage from the bulk draw solution through the membrane active layer and into the feed, was also calculated to determinethe draw solution losses during the forward osmosis process. It is helpful to compensate the draw solution directly with the concentrated draw solution in order not to decrease or lose the osmotic pressure driving force to keep the water flux stabilized. The ability of the forward osmosis membrane to reduce losses of draw solute is represented by the specific reverse solute selectivity (SRSF) [55]. The SRSF is necessary to calculate the replenishment costs of the draw solution, and it is shown in Fig. 17 that for each water liter recovered amount salt is lost towards the feed water. It was noticed that the specific reverse salt diffusion is increased with the increase of both water flux and solute reverse flux; the TFNC-0.4% (0.26 g/L) (AL-DS) (0.16 g/L) AL-FW shows a higher specific reverse salt diffusion compared to TFC membrane (0.22 g/L) (AL-DS) (0.14 g/L) (AL-FW).

Energy requirements for the seawater desalination forward osmosis process (FO-only) were evaluated using Eq. (9). It was noticed that the (Es-FO) decreased with increasing concentration of the draw solution for both membrane orientations,whichwas attributed to the increasing of the driving force between the draw solution and feed water. Also, the power consumption of FO (Es-FO) was lower in TFNC membranes compared to the TFC membrane that could be attributed to increasing water flux resulting from the addition of the zeolite nanoparticles in the TFNC membrane substrate. Moreover, the power

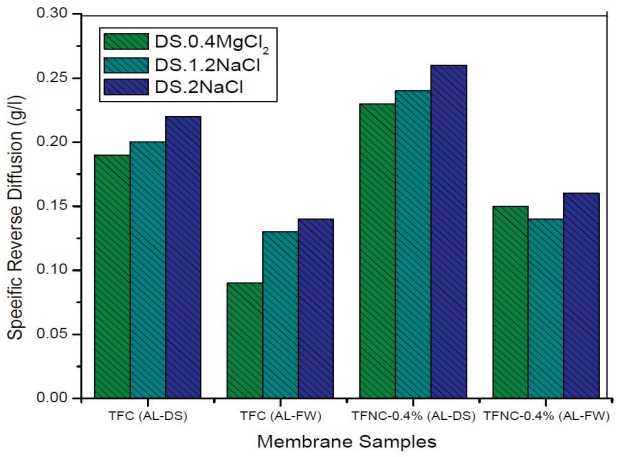

Fig. 17. Specific reverse salt diffusion for both draw solutions for both TFC and TFNC-0.4% membranes at different orientations (Test condition: 6 psi, 0.4 lpm, 25°C) (feed water, distilled water).

consumption increases as the feed salinity increasefrom the lower feed salinities (Brackish water) to the higher feed salinities (seawater). As stated in Figs. 18a and b, the lowest power consumption was achieved by using 2 M NaCl as a draw solution, followed by the 1.2 M NaCl and 0.4 $MgCl_2$.This is due to the higher effective osmotic pressure provided by the 2 M NaCl, which increases the water flux but, it will be atthe expense of increasing losses of the draw solution as stated in Fig. 16. Moreover, it should be mentioned that the magnesium chloride could not be used for higher seawater salinities as it could not reach a concentration higher than 0.4 M (practically), which provides a lower effective osmotic pressure (29 bar) so, it was evaluated with seawater salinity 25,000 ppm (21 bar). Itcould not be used for higher salinities as the power consumption will be very high compared to the sodium chloride, and it could reach the flux reversal point where the process of the FO will be reversed as the feed solution will have the effective driving force leading the water from the draw solution to the feed water.

The power consumption percentage of the forward osmosis process% Es-FO wasevaluated for both draw solution concentrations of NaCl (1.2 M and 2 M) as shown in Figs. 19 and 20a and b using both membrane orientations with respect to the total power consumption for RO in anS-WRO module.The power consumption for the RO module was evaluated using reverse osmosis system analysis (ROSA) for an existing plant in Hurghada, Red Sea, Egypt, Fig. 21. This is achievedby using Dow Dupont seawater membranes SW30HRLE-440 which is operated with recovery 34% as a standard recovery for the RO modulesfor an RO unit 500 m^3/d that used for the case study showing that the specific power consumption for the RO, $E_{S\text{-}RO}$ is 6.84 kWh/m^3 with pump efficiency 80% and feed pressure 67 bar (without using energy recovery device). Moreover, the energy recovery module was used to calculate the power consumption of the SWRO unit using the energy recovery device (PX Module)(Fig. 22). The specific power consumption $E_{S\text{-}RO}$ of the RO module is reduced to 3.69 kWh/m^3. The results showed that the power consumption in the FO process was only from 0.72% to 2.33% from $E_{S\text{-}RO}$by using 2 M draw solution for both membrane orientations for TFC and TFNC membranes, and from 1.52% to 4.66% $E_{S\text{-}RO}$ whenusing 1.2 M draw solution for both membrane orientations for TFC and TFNC membranes without using the energy recovery module in the RO. On the other side, by using the energy recovery device ERD, results stated that the power

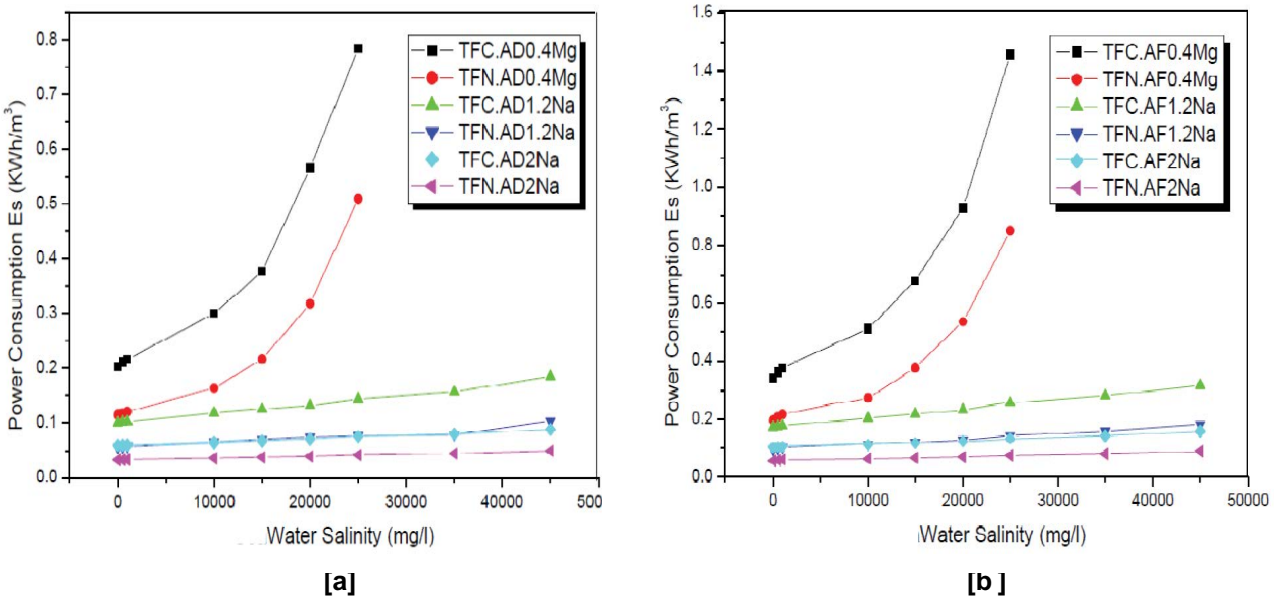

Fig. 18. (a and b) Specific power consumption for FO membranes for both TFC/TFNC-0.4 membranes at different SW salinities (Test condition: 6 psi, 0.4 lpm, 25°C (AL-D/FW) (Pump η 80%).

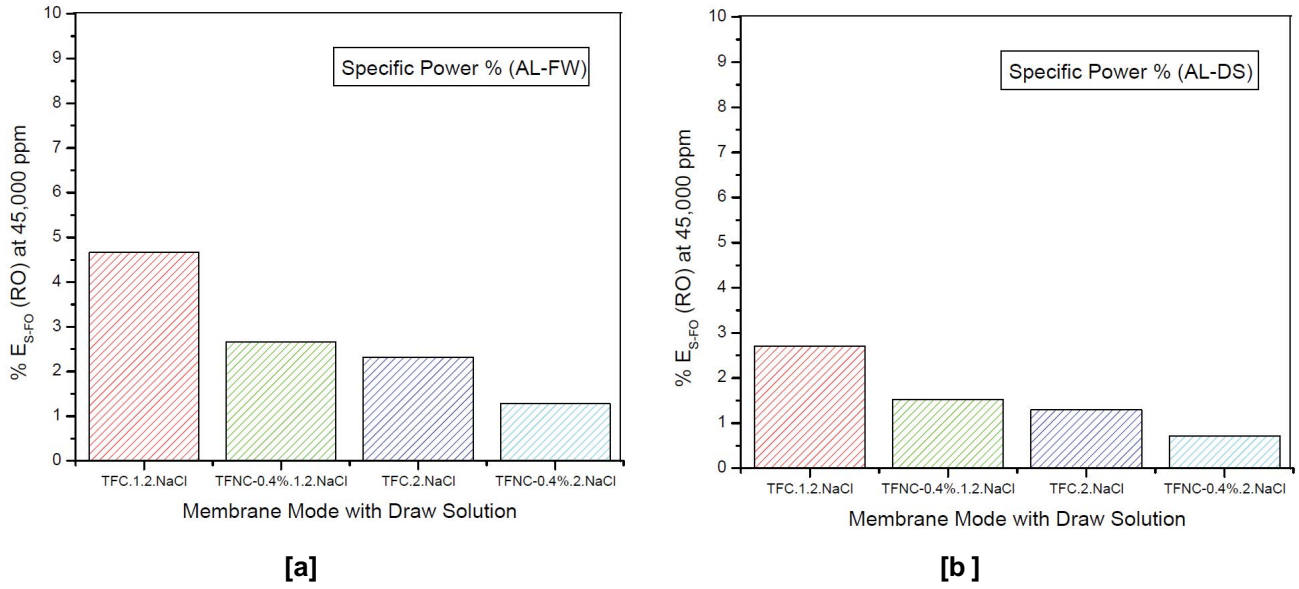

Fig. 19. (a and b) Specific power consumption percentage for FO membranes for both TFC/TFNC-0.4 membranes at different SW salinities W/O. ERD (Test condition: 6 psi, 0.4 lpm, 25°C) (AL-D/FW) (Pump η 80%).

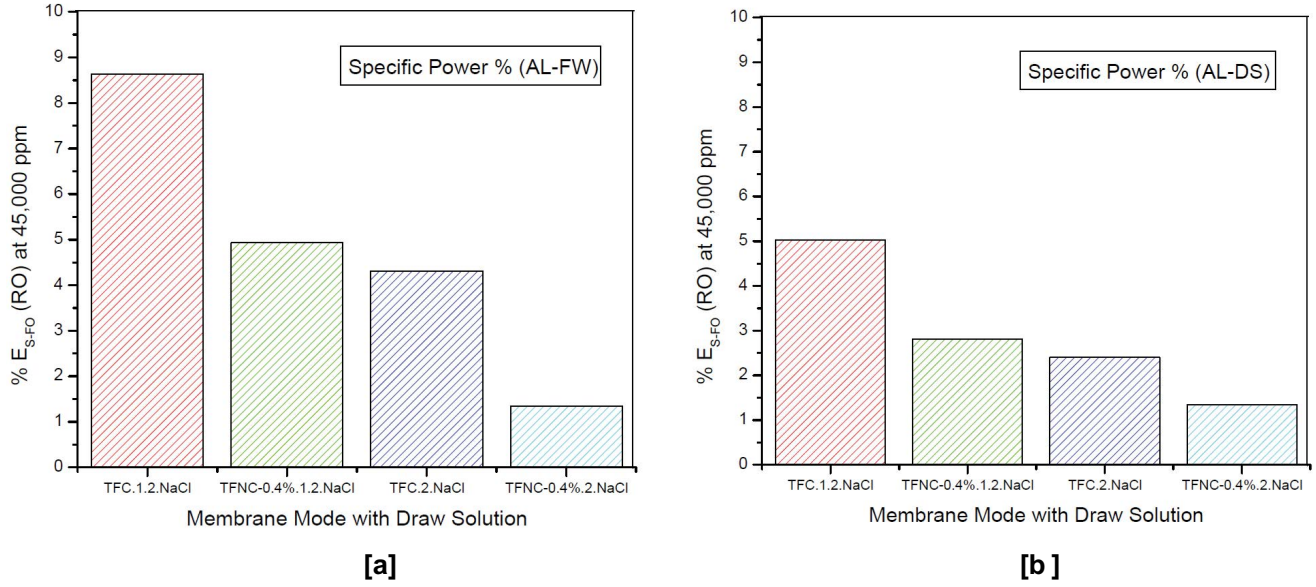

Fig. 20. (a and b) Specific power consumption percentage for FO membranes for both TFC/TFNC-0.4 membranes at different SW salinities W. ERD (Test condition: 6 psi, 0.4 lpm, 25°C) (AL-D/FW) (Pump η 80%).

consumption in the FO process was only from 1.3% to 4.3% from $E_{S\text{-}RO}$ by using 2 M draw solution for both membrane orientations for TFC and TFNC membranes and from 2.81% to 8.63% from $E_{S\text{-}RO}$ by using 1.2 M draw solution for both membrane orientations for TFC and TFNC membranes as shown in Tables 7 and 8 for brackish water to seawater salinities. It was reported that the average production cost of desalinated water in Egypt based on [SWRO + ERD-PX] with salinity [45,000 ppm] is 8 EGP/m^3 [0.51 $/$m^3$].It is taking into account the power, which represents about 70% of the total OPEX as shown in Table 9 [i.e., 5.53 EGP/m^3] [based on average power cost 1.5 EGP/kW], which means that the FO desalination process only could reduce the overall power cost to [0.072 – 0.132 EGP/m^3] Fig. 23is based on different membrane orientations for TFNC-0.4%.

The cost for the expensive regeneration process for the draw solution recovery is a significantpart that must be combined withthe overall seawater desalination cost disregarding the type of the draw solutionused [56]. Sodium chloride as a draw solution shows a good water flux in the FO module at high concentrations. However, these high concentrations could not be regenerated by the traditional RO modules as it will need a high pressure that exceeds the design pressure of most RO membranes and equipment as

Project Information: Forward Osmosis/RO

Case-specific:

System Details

Feed Flow to Stage 1	61.76 m³/h	Pass 1 Permeate Flow	21.00 m³/h	Osmotic Pressure:	
Raw Water Flow to System	61.76 m³/h	Pass 1 Recovery	34.00 %	Feed	35.82 bar
Feed Pressure	67.00 bar	Feed Temperature	25.0 C	Concentrate	55.66 bar
Flow Factor	0.85	Feed TDS	45036.84 mg/l	Average	45.74 bar
Chem. Dose (100% H2SO4)	0.00 mg/l	Number of Elements	36	Average NDP	20.37 bar
Total Active Area	1471.54 M²	Average Pass 1 Flux	14.27 lmh	Power	143.72 kW
Water Classification: Surface Supply SDI < 3				Specific Energy	6.84 kWh/m³

Stage	Element	#PV	#Ele	Feed Flow (m³/h)	Feed Press (bar)	Recirc Flow (m³/h)	Conc Flow (m³/h)	Conc Press (bar)	Perm Flow (m³/h)	Avg Flux (lmh)	Perm Press (bar)	Boost Press (bar)	Perm TDS (mg/l)
1	SW30HRLE-440i	6	6	61.76	66.66	0.00	40.76	65.18	21.00	14.27	0.00	0.00	230.75

Fig. 21. Membrane projection by ROSA for an RO unit 500 m³/d fed by a seawater 45,000 ppm with recovery rate 34%.

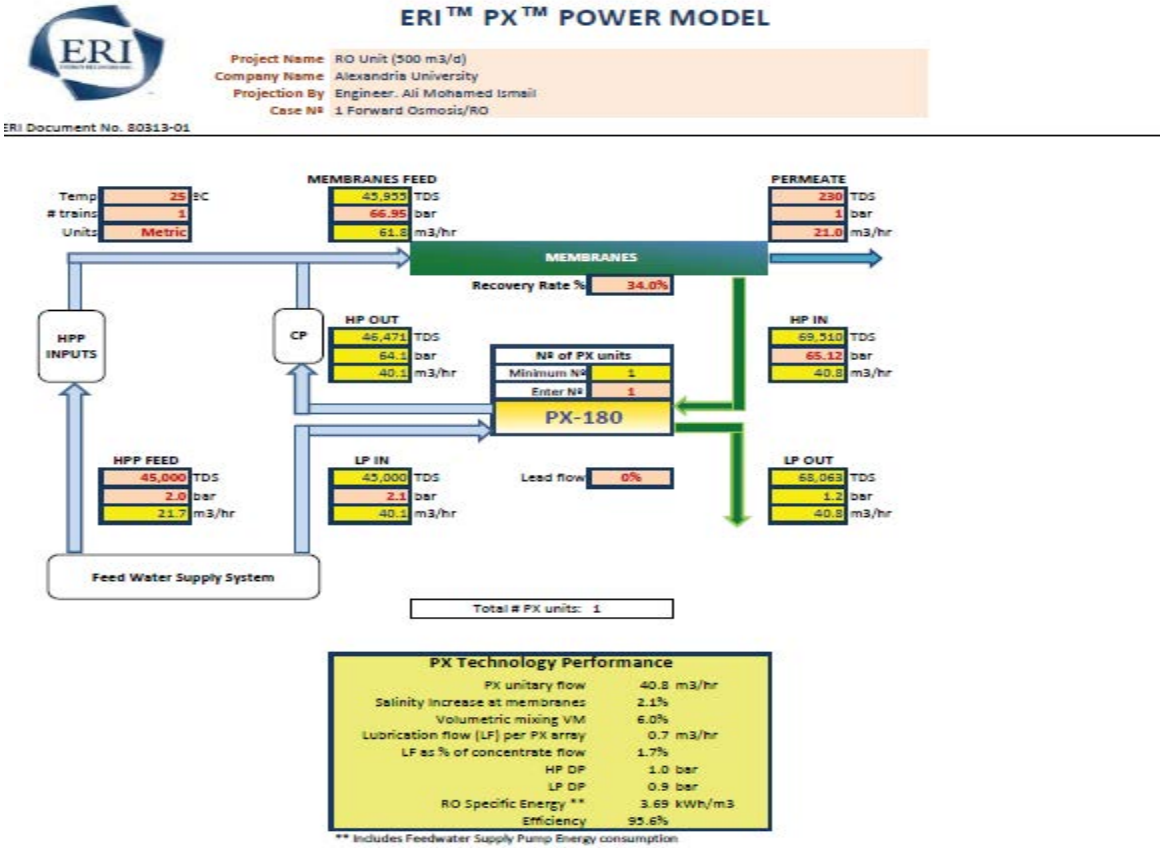

Fig. 22. RO energy recovery module by ERI for an RO unit 500 m³/d fed by a seawater 45,000 ppm with recovery rate 34%.

it may reach more than 140 bar for both the 1.2 and 2 M NaCl solutions. However, it could be used as a draw solution whenits concentration decreases so it will be able to be treated with the traditional RO modules but, it will be at the expense of reducing the water flux due to decreasing of the effective driving force between the draw solution and the feed water to the FO.

4. Conclusions

The current study evaluated the feasibility of the FO-RO hybrid process compared to RO for seawater desalination processes. First, practical FO experiments were used to assessthe performance of the FO and PSF substrate characteristics of the TFNC. FO membranes were effectively

Table 7
Specific power consumption percentage $E_{S\text{-}FO}/E_{S\text{-}RO}$ (W. ERD) (AL-DS)

Membrane orientations/ feed salinity	Specific power consumption percentage $E_{S\text{-}FO}/E_{S\text{-}RO}$ (W.ERD) (AL-DS)			
	TFNC-0.4% $E_{S\text{-}FO}$ [2 M]	TFC $E_{S\text{-}FO}$ [2 M]	TFNC-0.4% $E_{S\text{-}FO}$ [1.2 M]	TFC $E_{S\text{-}FO}$ [1.2 M]
500 ppm	0.48%	0.87%	0.82%	1.49%
1000 ppm	0.49%	0.87%	0.84%	1.5%
10,000 ppm	0.52%	0.94%	0.94%	1.73%
20,000 ppm	0.57%	1.03%	1.08%	1.93%
35,0000 ppm	0.65%	1.17%	1.15%	2.29%
45,000 ppm	0.72%	1.29%	1.52%	2.71%

Table 8
Specific power consumption percentage $E_{S\text{-}FO}/_{ES\text{-}RO}$ (W. ERD) (AL-FW)

Membrane orientations/ feed salinity	Specific power consumption percentage $E_{S\text{-}FO}/E_{S\text{-}RO}$ (W.ERD)(AL-FW)			
	TFNC-0.4% $E_{S\text{-}FO}$ [2 M]	TFC $E_{S\text{-}FO}$ [2 M]	TFNC-0.4% $E_{S\text{-}FO}$ [1.2 M]	TFC $E_{S\text{-}FO}$ [1.2 M]
500 ppm	0.84%	1.52%	1.43%	2.55%
1000 ppm	0.86%	1.53%	1.47%	2.6%
10,000 ppm	0.91%	1.63%	1.65%	2.98%
20,000 ppm	1%	1.79%	1.88%	3.3%
35,0000 ppm	1.15%	2%	2.32%	4.14%
45,000 ppm	1.28%	2.32%	2.66%	4.66%

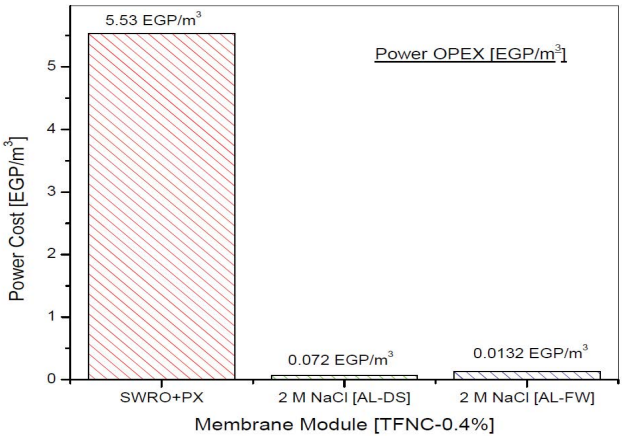

Fig. 23. Power OPEX comparison between current SWRO-ERD and TFNC-0.4% membranes.

Table 9
OPEX Percentage for SWRO/ERD 500 m^3/d

OPEX	Percentage
Power cost	70%
Materials & spares	15%
Labor salaries	10%
Medical, social, insurance	3%
Others	2%

modified by mingling different concentrations of zeolite nanoparticles from 0 to 0.6 wt% within the polysulfone matrix, increasing the hydrophilicity and porosity of the nanocomposite substrate,which directly affect the water flux. Then, the regeneration process was evaluated using reverse osmosis system analysis for an existing SWRO+PX unit in Hurghada, RedSea, Egypt.The TFNC-0.4% membrane prepared from PSF substrate implanted with (0.4 wt%) zeolite nanoparticles exhibited the best performance among other concentrations by increasing the water flux by 126% than the TFC membranes. Practical experiments showed that in the forward osmosis experiments, the (AL-DS) membrane orientations showed a higher water flux than that of (AL-FW) but accompanied with higher solute reverse flux.

Although higher fluxes are reached with the increaseof draw solution concentration, the power cost of the desalination process tends to increase with the increase in the draw solution concentration. Moreover, the increase in zeolite concentrations in the polysulfone substrate increases the water flux for the TFNC membranes, while salt rejection is decreased at high concentrations. This is attributed to the lower degree of cross-linking of the polyamide selective layer formed. Dissolved inorganic salts remain the most effective draw solutes due to their high osmotic pressure that driveswater permeation through the membrane. The power consumption in the promising forward osmosis technology alone was a small percentage of (0.72 to 4.66%) of the total power consumption in the RO process, which reduces the power OPEX for theSWRO+PX with 45,000 ppm from 5.53 EGP/m^3 to 0.072 EGP/m^3].Therefore, most of the FO-RO process power consumption was realized in the RO regeneration process.The FO-RO hybrid water desalination

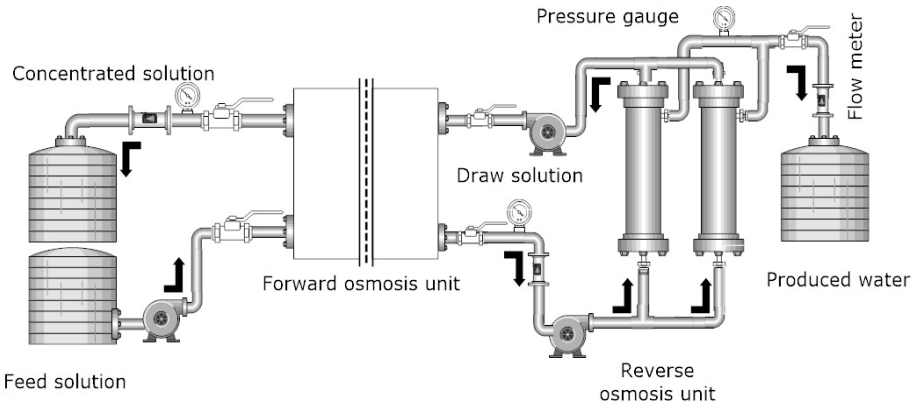

Fig. 24. Proposed FO-RO hybrid system desalination module.

module is not consuming lower energy than a standalone RO module to achieve a specificrecovery. However, the FO advantage is that it could work as a pretreatment for the conventional RO system to increase the lifetime of the RO membrane and reduce the frequencies of chemical cleaning and the usage of scale inhibitors for RO membranes (Fig. 24). Although the divalent salts consume much lower power in the regeneration process as a draw solution, they cannot be used as they have a very low osmotic pressure and their practical solubility limits are very low compared to the monovalent salts. The synthesized TFNC-0.4% nanocomposite membrane will have broad applications in the FO seawater desalination by innovative draw solution with economic recovery solution.According tothe results achieved in this study, it can be concluded that forward osmosis polysulfone membrane substrate impeded with proper zeolite nanoparticles could potentially improve the overall performance of FO desalination processes by enhancing desalination power OPEX to make the forward osmosis economically feasible.

Acknowledgment

The authors are grateful to the Egyptian Desalination Research Center of Excellence, Desert Research Center, Egypt, Chemical Engineering Dept, Alexandria University, Dr. Zaki Youssef Girgis, Prof. Dr. Mohamed Ismail for the support which helps to accomplish this study.

Symbols

A	—	Pure water permeability (A), L/m² h bar
A_m	—	Membrane active surface area, m²
B	—	Salt permeability coefficient, L/m² hr
C_f	—	Salt concentration in the feed solution, ppm
C_d	—	Salt concentration in the draw solution, ppm
C_p	—	Salt concentration in the permeate, ppm
$E_{s\text{-}FO}$	—	Specific power consumption for forward osmosis, kWh/m³
$E_{s\text{-}RO}$	—	Specific power consumption for reverse osmosis, kWh/m³
E_{st}	—	Total power consumption of both FO/RO processes, kWh/m³
I	—	Van't Hoff Constant, dimensionless
J_s	—	Reverse salt (solute) flux, g/m² h
J_w^{RO}	—	Pure water flux based on RO, L/m² h
J_v	—	Pure water flux based on FO, L/m² h
P	—	Membrane applied pressure, bar
P_f	—	Feed solution pressure, bar
P_{ds}	—	Draw solution feed pressure, bar
Q_p	—	Permeate flow rate, m³/h
$Q_{sw\text{-}in}$	—	Inlet flow rates for feed water, m³/h
$Q_{ds\text{-}in}$	—	Inlet flow rates for draw solution, m³/h
OPEX	—	Operating expenses
R	—	Universal gas constant, L atm/mole K
R	—	Salt rejection, %
S	—	Membrane structural parameter, dimensionless
t	—	Operation time, h
T	—	Operation temperature, K
V	—	Permeate volume, L
W_w	—	Weight of wet membrane, g
W_d	—	Weight of dry membrane, g
ρ	—	Solution density, kg/m³
ε	—	Membrane porosity, %
π	—	Osmotic pressure in, atm
η	—	Pump efficiency, %

References

[1] M. Abdullah, M. Man, P. Nyan, S. Saufi, S. Abdullah, Potential thermoresponsive ionic liquid as draw solution in forward osmosis application, J. Eng. Sci. Technol., 2 (2019) 1031–1042.
[2] J. Puguan, H. Kim, K. Lee, H. Kim, Low internal concentration polarization in forward osmosis membranes with hydrophilic crosslinked PVA nanofibers as porous support layer, Desalination, 336 (2014) 21–31.
[3] S. Sikdar, What about industrial water sustainability? Clean Technol. Environ. Policy, 13 (2011) 13.
[4] A. Mollahosseini, A. Abdderasoul, Recent advances in thin film composites membrane for brackish ground water treatment with critical focus on Saskatchewan water sources, J. Environ. Sci., 81 (2019) 181–194.
[5] B. Bruggen, P. Luis, Forward osmosis: understanding the hype, DE Gruyter, Rev. Chem. Eng., 31 (2015) 1–12.

[6] I. Ibrar, A. Altaee, J. Zhou, O. Naji, D. Khanafer, Challenges and potentials of forward osmosis process in the treatment of wastewater, critical reviews, Environ. Sci. Technol., 50 (2020) 1339–1383.
[7] T.S. Chung, X. Li, R.C. Ong, Q. Ge, H.L. Wang, G. Han, Emerging forward osmosis (FO) technologies and challenges ahead for clean water and clean energy applications, Curr. Opin. Chem. Eng., 1 (2012) 246–257.
[8] J. Wei, X. Liu, C. Qiu, R. Wang, C.Y. Tang, Influence of monomer concentrations on the performance of polyamide-based thin film composite forward osmosis membranes, J. Membr. Sci., 381 (2011) 110–117.
[9] X. Liu, S. Qi, Y. Li, L. Yang, B. Cao, C.Y. Tang, Synthesis and characterization of novel antibacterial silver nanocomposite nanofiltration and forward osmosis membranes based on layer-by-layer assembly, Water Res., 47 (2013) 3081–3092.
[10] A. Tiraferri, N.Y. Yip, W.A. Phillip, J.D. Schiffman, M. Elimelech, Relating performance of thin-film composite forward osmosis membranes to support layer formation and structure, J. Membr. Sci., 367 (2011) 340–352.
[11] J. Li, Z. Xu, H.Yang, L. Yun, M. Liu, Effect of TiO_2 nanoparticles on the surface morpohology and perofrmance of microporous PES membrane, Appl. Surf. Sci., 255 (2009) 4725–4732.
[12] D. Emadzadeh, W.J. Lau, T. Matsuura, M. Rahbarie-Sisakht, A.F. Ismail, A Novel thin film composite forward osmosis membrane prepared from PSF-TiO_2 nanocomposite substrate for water desalination, Chem. Eng. J., 237 (2014) 70–80.
[13] H. Shawky, R. Yassen, Y.H. Kotb, D. Eissa, Biosynthesis of silver nanoparticles and its effect in TFC RO membrane for ground water desalination, Desal. Water Treat., 193 (2020) 34–47.
[14] A.H. Konsowa, S.H. Kandil, R. Gaber, M.G. Eloffy, S.M. Ebrahim, The effect of coagulation time on the performance of thin film composite RO membrane casted on non-woven polyester, Desal. Water Treat., 147 (2019) 38–45.
[15] A. Rahimpour, M. Jahanshahi, A. Mollahosseini, B. Rajaeian, Structural andperformance properties of UV-assisted TiO_2 deposited nano-composite PVDF/SPES membranes, Desalination, 285 (2012) 31–38.
[16] S. Loeb, G.D. Mehta, A two-coefficient water transport equation for pressure retarded osmosis, J. Membr. Sci., 4 (1978) 351–362.
[17] D. Emadzadeh, W.J. Lau,T. Matsuura, A.F. Ismail, M. Rahbari-Sisakht, Synthesis and characterization of thin film nanocomposite forward osmosis membrane with hydrophilic nanocomposite support to reduce the internal concentration polarization, J. Membr. Sci., 449 (2014) 74–85.
[18] A. Altaee, G. Zaragoza, H. Rost, V. Tonningen,Comparison between forward osmosis-reverse osmosis processes for seawater desalination, Desalination, 336 (2014) 50–57.
[19] N. Ma, J. Wei, R. Liao, C.Y. Tang, Zeolite-polyamide thin film nanocomposite membranes: towards enhanced performance for forward osmosis, J. Membr. Sci., 405 (2012) 149–157.
[20] Y. Kotp, High-flux TFN nanofiltration membranes incorporated with Camphor-Al_2O_3 nanoparticles for brackish water desalination, Chemosphere, 265 (2021) 128999.
[21] E. Drioli, L. Giorno, E. Fontananova, Comprehensive Membrane Science and Engineering, Elsevier, 2017.
[22] N. Widjojo, T. Chung, M. Weber, C. Maletzko, V. Warzelhan, The role of sulphonated polymer and macrovid-free structure in the support layer for thin-film composite (TFC) forward osmosis (FO) membranes, J. Membr. Sci., 383 (2011) 214–223.
[23] G. Han, T. Chung, M. Toriida, S. Tamai, Thin-film composite forward osmosis membranes with novel hydrophilic supports for desalination, J. Membr. Sci., 423–424 (2012) 543–555.
[24] D.F. Li, T. Chung, J. Ren, R. Wang, Thickness dependance of macroviod evaluation in wet phase-inversion asymmetric membranes, Ind. Eng. Chem. Res., 43 (2004) 1553–1556.
[25] B. Tarboush, D. Rana, T. Matsuura, H. Arafat, R. Narbaitz, Preparation of thin film composite polyamide membranes for desalination using novel hydrophilic surface modifying macromolecules, J. Membr. Sci., 325 (2008) 166–175.
[26] H. Shawky, Performance of aromatic polyamide RO membranes synthesized by interfacial polycondensation process in a water tetrahydrofuran system, J. Membr. Sci., 339 (2009) 209–214.
[27] M. Naushad, Surfactant assisted nano-composite cation exchanger: development, characterization and applications for the removal of toxic Pb^{2+} from aqueous medium, Chem. Eng. J., 235 (2014) 100–108.
[28] M. Naushad, Z.A. AlOthman, Separation of toxic Pb^{2+} metal from aqueous solution using strongly acidic cation-exchange resin: analytical applications for the removal of metal ions from pharmaceutical formulation, Desal. Water Treat., 53 (2015) 2158–2166.
[29] H. Kasgoz, A. Durmus, A. Kasgoz, Enhanced swelling and adsorption properties of AAm-AMPSNa/clay hydrogel nanocomposites for heavy metal ion removal, Polym. Adv. Technol., 19 (2008) 213–220.
[30] M. Naushad, A. Mittal, M. Rathore, V. Gupta, Ion-exchange kinetic studies for Cd(II), Co(II), Cu(II), and Pb(II) metal ions over a composite cation exchanger, Desal. Water Treat., 54 (2015) 2883–2890.
[31] M. Naushad, Z.A. AlOthman, M.R. Awual, M.M. Alam, G.E. Eldesoky, Adsorbtion kinetics, isotherms, and thermo-dynamic studies for the adsorption of Pb^{2+} and Hg^{2+} metal ions from aqueous medium using Ti(IV) iodovanadate cation exchanger, Ionics (Kiel), 21 (2015) 2237–2245.
[32] M.A. Gomaa, A.A. Hamouda, M.E. Abdelfatah, M.M. Emara, M.M.B. El-Sabbah, The effect of nano-materials on the charactersitics and performaance of aromatic polyamide membranes and its use in groundwater desalination in the area between Safaga and El-Qusir, Egypt, J. Appl. Sci. Res., 9 (2013) 4709–4808.
[33] A. El-Assar, Moustafa M. Abo El Fadl, M. Ali, Y. Kotb, H. Shawky, Effect of manufacture conditions on reverse osmosis desalination performance of polyamide thin film composite membrane and their spiral wound element, Desal. Water Treat., 69 (2017) 65–71.
[34] G. Summers, M. Ndawuni, C. Summers, Dipyridyl function-alized polysulfones for membrane production, J. Membr. Sci., 226 (2003) 21–33.
[35] S. Villar- Rodil, J.I. Paredes, A. Alonso, J.M.D Tascon, Atomic force microscopy and infrared spectroscopy studies of the thermal degradation of nomex aramid fibers, Chem. Mater., 13 (2001) 4297–4304.
[36] M. Maghami, A. Abdelrasoul, Zeolite mixed matrix nanofiltration membranes for the next generation of water purification, Intechopen, (2018) 75083.
[37] Y. Yang, P. Wang, Q. Zheng, Preparation and properties of polysulfone/TiO_2 composite ultrafiltration membranes, J. Polym. Sci. Polym. Phys., 44 (2006) 879–887.
[38] M. Fathizadeh, A. Aroujalian A. Raisi, Effect of added NaX nano-zeolite into polyamide as a top thin layer of membrane on water flux and salt rejection in a reverse osmosis process, J. Membr. Sci., 375 (2011) 88–95.
[39] N. Hilal, M. Khayat, C.J. Wright, Membrane Modification: Technology and Applications, CRC Press, T. Francis Grp.: Boca Raton, FL, 2012.
[40] T. Sano, H. Yanagishita, Y. Kiyozumi, F. Mizukami, K. Haraya, Separation of ethanol/watermixture by silicalite membrane on pervaporation, J. Membr. Sci., 95 (1994) 221–228.
[41] Q. Liu, R. Noble, J. Falconer, H. Funke, Organics/water separation by pervaporationwith a zeolite membrane, J. Membr. Sci., 117 (1996) 163–174.
[42] T. Sano, S. Ejiri, K. Yamada, Y. Kawakami, H. Yanagishita, Separation of acetic acid-watermixtures by pervaporation through silicalite membrane, J. Membr. Sci., 123 (1997) 225–233.
[43] G.Ciobanu, G. Carja, O. Ciobanu, Structure of mixed matrix membranes made with SAPO-5 zeolite in polyurethane matrix, Microporous Mesoporous Mater., 115 (2008) 61–66.
[44] B. Jeong, E. Hoek, Y. Yan, A. Subramani, X. Huang, G. Hurwitz, A. Jawor, Interfacialpolymerization of thin film nanocomposites: a new concept for reverse osmosis membranes, J. Membr. Sci., 294 (2007) 1–7.
[45] V. Thang, H. Kaliaguine, Predictive models for mixed-matrix membrane performance: a review, Chem. Rev., 113 (2013) 4980–5028.

[46] J. Wei, C. Qiu, C. Tang, R. Wang, A. Fane, Synthesis and characterization of flat-sheet thin film composite forward osmosis membranes, J. Membr. Sci., 372 (2011) 292–302.
[47] W. Lay, J. Zhang, C. Tang, R. Wang, Y. Liu, A.G. Fane, Factors affecting fluxperformance of forward osmosis systems, J. Membr. Sci., 394 (2012) 151–168.
[48] N. Yip, A. Tiraferri, W. Philip, J.D. Schiffman, M. Elimelech, High performance thin-film composite forward osmosis membrane, Environ. Sci. Technol., 44 (2010) 3812–3818.
[49] I. Alvik, M.-B. Hagg, Pressure retarded osmosis and reverse osmosis membranes: materials and methods, Polymers, 5 (2013) 303–327.
[50] J. Ren, J.R. McCutcheon, A new commercial thin film composite membrane for forward osmosis, Desalination, 343 (2024) 187–193.
[51] N. Widjojo, T. Chung, M. Weber, C. Maletzko, V. Warzelhan, A sulfonatedpolyphenylenesulfone (SPPSU) as the supporting substrate in thin filmcomposite (TFC) membranes with enhanced performance for forwardosmosis (FO), Chem. Eng. J., 220 (2013) 15–23.
[52] K. Wang, T. Chung, G. Amy, Developing thin film composite forward osmosis membranes based on the PES/SPSF substrate through interfacial polymerization, AIChE J., 58 (2012) 770–781.
[53] C. Nayak, N. Rastogi, Forward osmosis for concentration of anthocyanin from Kokum (Garciana indica Choisy), Sep. Purif. Technol., 71 (2010) 144–151.
[54] B. Mi, M. Elimelech, Organic fouling of forward osmosis membranes: fouling reversibility and cleaning without chemical reagents, J. Membr. Sci., 348 (2010) 337–345.
[55] D. Shaffer, J. Werber, H. Jaramillo, S. Lin, M. Elimelech, Forward osmosis: where are we now, Desalination, (2014) 12318.
[56] A. Altaee, G.J. Millar, G. Zaragoza, A. Sharif, Energy effciency of RO and FO-RO system for high salinity seawater treatment, Clean Technol. Environ. Policy, 19 (2017) 77–91.